iScience

CellPress
OPEN ACCESS

Article

Exosomes derived from platelet-rich plasma promote diabetic wound healing via the JAK2/STAT3 pathway

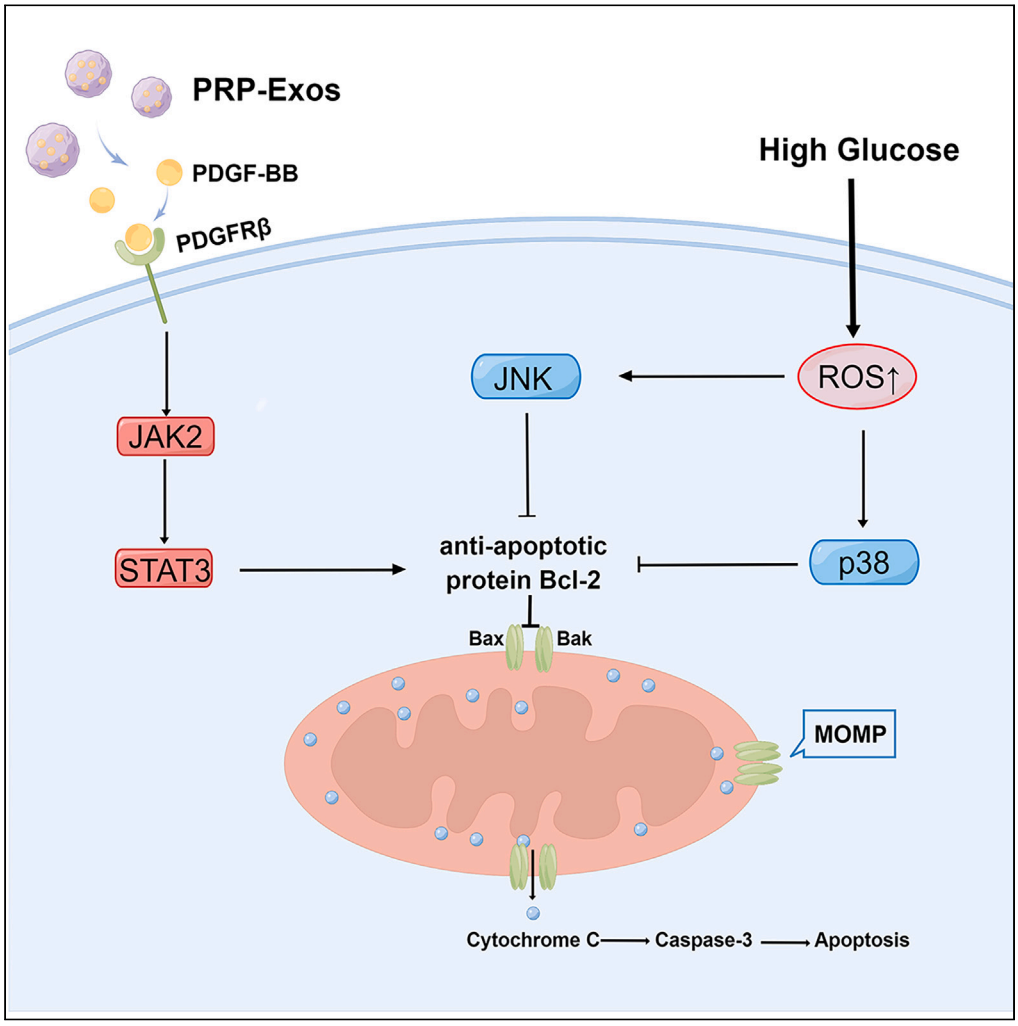

Wenhai Cao, Xiaotong Meng, Fangming Cao, Jinpeng Wang, Maowei Yang

mwyang@cmu.edu.cn

Highlights

PRP-Exos could promote fibroblasts proliferation and migration

PRP-Exos alleviate HG-induced apoptosis through JAK2/STAT3/Bcl-2 pathway

PRP-Exos have a protective effect on diabetic wound healing

Cao et al., iScience 26, 108236
November 17, 2023
https://doi.org/10.1016/j.isci.2023.108236

iScience

CellPress
OPEN ACCESS

Article

Exosomes derived from platelet-rich plasma promote diabetic wound healing via the JAK2/STAT3 pathway

Wenhai Cao,[1,2,3] Xiaotong Meng,[1,2] Fangming Cao,[1] Jinpeng Wang,[1] and Maowei Yang[1,*]

SUMMARY

Diabetic non-healing wounds are bringing a heavy burden on patients and society. Platelet-rich plasma (PRP) has been widely applied in tissue regenerating for containing various growth factors. Recently, PRP-derived exosomes (PRP-Exos) have been proved to be more effective than PRP in tissue regeneration. However, few studies have investigated the therapeutic potential of PRP-Exos in diabetic wound healing to date. Therefore, we extracted and identified exosomes derived from PRP and tested its promoting effect on diabetic wound healing *in vivo* and *in vitro*. We found that high glucose (HG) inhibited cell proliferation and migration and induced apoptosis through ROS-dependent activation of the JNK and p38 MAPK signaling pathways. PRP-Exos can stimulate fibroblast functions and accelerate diabetic wound healing. The benefits of PRP-Exos may be attributed to its capability to prevent HG-induced ROS-dependent apoptosis via the PDGF-BB/JAK2/STAT3/Bcl-2 signaling pathway. This illustrates the therapeutic potential of PRP-Exos in diabetic wounds.

INTRODUCTION

The prevalence of diabetes mellitus (DM) and its relevant complications are on the rise around the world, with serious consequences for patients and healthcare systems. Among the complications, a major concern for public health is chronic wounds caused by diabetes.[1] Normal wound healing involves phases of inflammation, proliferation, and tissue remodeling.[2] As the wound heals, fibroblasts are present from the late inflammatory stage to full epithelization.[3] Fibroblasts proliferate in the wound and synthesize extracellular matrix (ECM), which regulates and provides support for the activity of fibroblasts. Meanwhile, ECM also supports and transfers signals to accelerate granulation tissue generation, angiogenesis, and epithelialization.[4] In diabetes, wound healing is a complex process consisting of various biochemical and molecular events, and diabetes influences wound healing at all stages. The occurrence and development of diabetic wounds are believed to be largely influenced by oxidative stress.[5] A highly oxidizing environment, which is associated with hyperglycemia, leads to apoptosis of fibroblasts, causing insufficient synthesis of ECM, excessive activation of proteolytic activity, attenuated wound contraction, and finally, a nonhealing wound.[6]

Over the last decades, new advanced therapies have been developed to address compromised wounds. Platelet-rich plasma (PRP), as a product obtained by autologous blood centrifugation, contains supraphysiological concentrations of platelets and growth factors.[7] A variety of pro-tissue-healing growth factors and cytokines can be released by degranulated platelets.[8] There is great potential for PRP to enhance skin healing because it contains molecules and cytokines such as VEGF (vascular endothelial growth factor), PDGF (platelet-derived growth factor), and TGF-β (transforming growth factor β) that promote collagen synthesis, angiogenesis, or cellular proliferation as well as the deposition of ECM.[9,10] Despite all of these benefits, the requirement for autologous platelets, complicated preparation procedures, and the lack of standardized protocols for preparation limit the popularization of PRP.[11]

In addition to growth factors, platelets secrete several extracellular vesicles, including exosomes, upon stimulation. Exosomes, which are 40–150 nm in size and of endosomal origin, are believed to be essential for intercellular communication by delivering bioactive proteins and RNA to recipient cells.[12] Moreover, due to their low immunogenicity and stability, exosomes can carry signals across species.[13] With their capacity to transport large cargo loads, exosomes have become the preferred carrier of clinical nanomedicine due to their ability to protect biomolecules from destructive enzymes and chemicals.[14] Since Torreggiani et al.[15] first extracted exosomes from PRP in 2014, PRP-derived exosomes (PRP-Exos) have been confirmed to promote tissue repair and regeneration.[16–20] However, several of the studies mainly on wound healing did not discuss in detail the inhibitory effect of diabetes on wound healing both *in vivo* and *in vitro* simultaneously and failed to further explore the specific mechanism of exosomes on wound healing in a diabetic environment. Therefore, we decided to use a high-glucose environment *in vitro* to simulate the effect of the diabetic environment on fibroblasts and to test the therapeutic ability of exosomes in a diabetic rat model *in vivo*.

[1]Department of Orthopedics, First Hospital of China Medical University, Shenyang, China
[2]These authors contributed equally
[3]Lead contact
*Correspondence: mwyang@cmu.edu.cn
https://doi.org/10.1016/j.isci.2023.108236

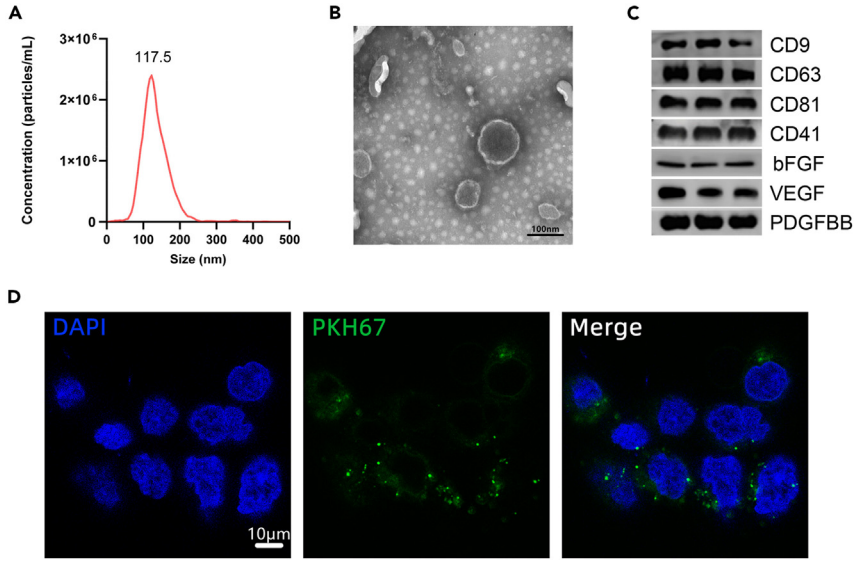

Figure 1. Characterization of PRP-Exos

(A) Particle size distribution measured by DLS.

(B) Morphology observed by transmission electron microscopy. Scale bar: 100 nm.

(C) Western blotting analysis of the exosome surface markers and cargo.

(D) Fluorescence staining results of PKH67-labeled PRP-Exos co-cultured with HSFs; green represents PKH67, and blue represents nuclear DNAs stained by DAPI. Scale bar: 10 μm.

Based on the facts mentioned earlier, we studied the influence of high glucose on fibroblasts and whether PRP-Exos could exert a protective effect. Furthermore, the molecular mechanism underlying the function of PRP-Exos was investigated. We also applied a biocompatible HP-PEG/HA-SH hydrogel to test the effect of the hydrogel and PRP-Exos on diabetic wounds when applied alone and in combination through animal experiments. To our knowledge, we are the first to investigate the effect of PRP-Exos on protecting fibroblasts from the high-glucose environment *in vitro* and promoting diabetic wound healing *in vivo* simultaneously.

RESULTS

Identification of exosomes and biological effects

Characterization of PRP-Exos

Purified nanoparticles derived from PRP were identified using Nanosight tracking analysis (NTA), transmission electron microscopy (TEM), and western blotting. NTA showed that the peak size of the particles was 117.5 nm (Figure 1A). The exosomes appeared to be cup-shaped or sphere-shaped with a diameter of approximately 100 nm, as observed by TEM (Figure 1B). The WB results confirmed that PRP-Exos exhibited high expression of the Exo markers CD9, CD63, and CD81 and the source marker of platelet CD41 (Figure 1C). All of these results indicated the existence of Exo. In addition, PDGFBB, VEGF, and bFGF were confirmed in the exosome cargo (Figure 1C).

PRP-Exos could be internalized by HSFs

Next, we found that fibroblasts internalized PRP-Exos. PRP-Exos were labeled with the fluorescent dye PKH67 (green) and incubated with fibroblasts. After 24 h, recipient cells were stained with DAPI. HSFs were found to have taken up PKH67-labeled exosomes by fluorescence microscopy (Figure 1D).

PRP-Exos promoted the proliferation and migration of HSFs

Cell proliferation and migration were assessed by culturing HSFs in conditioned medium supplemented with different concentrations of PRP-Exos. The proliferation activity was evaluated by CCK-8 assays at 24, 48, and 72 h, and the results indicated that PRP-Exos significantly promoted HSF proliferation (Figure 2A). For the 50 μg/mL and 100 μg/mL groups, differences were observed starting at 24 h compared with the control group, but there were no differences between the two groups. For the 5 μg/mL PRP-Exos group, differences were observed starting at 48 h.

Migration was investigated by Transwell and scratch wound assays (Figures 2B and 2C). The exosomes were able to promote the migration of fibroblasts in a dose-dependent manner in both Transwell and scratch wound assays (Figures 2D and 2E).

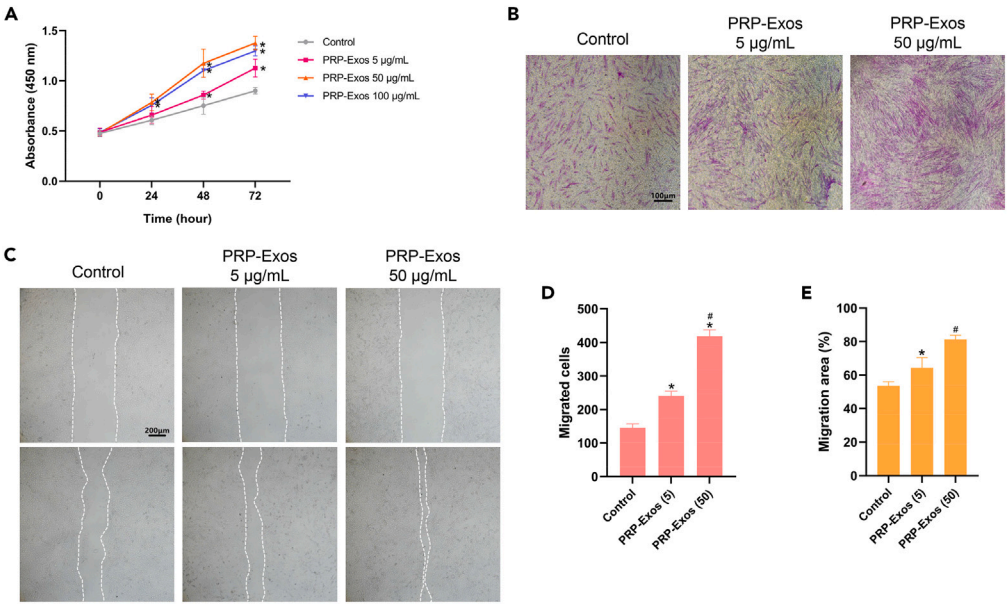

Figure 2. Effects of PRP-Exos on cell proliferation and migration

(A) Different concentration of PRP-Exos promoted the proliferation of fibroblasts, analyzed by CCK-8 assay.

(B) Representative photomicrographs showing the effect of PRP-Exos on the Transwell migration (violet-stained cells) of HSFs. Scale bar: 100 μm.

(C) The effect of PRP-Exos on migration of HSFs analyzed by scratch wound assay. Scale bar: 200 μm.

(D and E) Quantitative analysis of the Transwell assays and scratch wound assays. *$p < 0.05$ compared with control. #$p < 0.05$ comparing PRP-Exos (5) and PRP-Exos (50).

PRP-Exos alleviated HG-induced apoptosis and inhibited proliferation and migration

To mimic the hyperglycemic condition of diabetes *in vitro*, HSFs were exposed to different concentrations of glucose to investigate the impact of high glucose through CCK-8 and Annexin V-FITC/PI assays (Figures 3A–3C). The results of the CCK-8 assays showed that cell proliferation was compromised under 35, 45, and 55 mM glucose in a dose-dependent manner, and the results for cell apoptosis were similar. Based on these results, we used HG (55 mM) with or without PRP-Exos (50 μg/mL) for 48 h in the following experiments if not stated otherwise.

In further analysis, the negative effect of HG was attenuated by PRP-Exos. The inhibition of proliferation was rescued by exosomes through the CCK-8 assay (Figure 3F), and the alleviation of migration was confirmed by the Transwell assay (Figures 3D and 3E) and wound scratch assay (Figures 3G and 3H). The Annexin V-FITC/PI assay indicated that PRP-Exos could alleviate cell apoptosis induced by HG without affecting cell apoptosis when used alone (Figures 3I and 3J).

PRP-Exos alleviated HG-induced apoptosis through PDGF-BB/JAK2/STAT3 pathway

HG triggered the intrinsic apoptosis pathway through the ROS-dependent JNK and p38 pathways

The intrinsic apoptosis pathway, or mitochondrial pathway, is primarily characterized by mitochondrial dysfunction and is widely involved in the pathogenesis of diabetic complications.[21] Hyperglycemia is believed to induce oxidative stress through various pathways and then lead to activation of the mitochondrial apoptosis pathway.[22] Therefore, we investigated whether HG triggers the intrinsic apoptosis pathway by inducing intracellular ROS overproduction. First, we discovered that ROS could be induced by HG as deduced by the ROS scavenger NAC through fluorescence microscopy and flow cytometry (Figures 4A, 4B, 4D, and 4E). Mitochondrial membrane potential ($\Delta\Psi m$) loss in the HG group was also observed via JC-1 staining detected by flow cytometry, and it could be reversed by NAC (Figures 4C and 4F). The expression of SOD 1 and CAT, two kinds of essential antioxidant proteins, presented similar results on western blotting (Figure 4G). All of these findings demonstrated that HG could result in oxidative stress and mitochondrial outer membrane permeabilization (MOMP).

The JNK and p38 MAPK signaling pathways play key roles in cellular apoptosis in response to extracellular signals and stress.[23] Our next step was to determine whether the JNK and p38 MAPK pathways participate in HG-induced apoptosis. The WB results showed that HG markedly increased both JNK and p38 protein phosphorylation, increased expression of the pro-apoptotic protein Bax and executive protein cleaved caspase-3, and inhibited the expression of anti-apoptotic protein Bcl-2. The ROS scavenger NAC almost completely neutralized the apoptosis activated by HG, whereas the JNK inhibitor SP600125 and the p38 inhibitor SB203580 partly decreased the proapoptotic function of HG (Figures 4H–4L). The involvement of the JNK and p38 MAPK pathways in HG-mediated apoptosis was also validated by an Annexin V-FITC/PI detection assay. The data showed that NAC (ROS scavenger), SP600125 (JNK inhibitor), and SB203580 (p38 inhibitor) all inhibited apoptosis in an HG environment (Figures 4M and 4N).

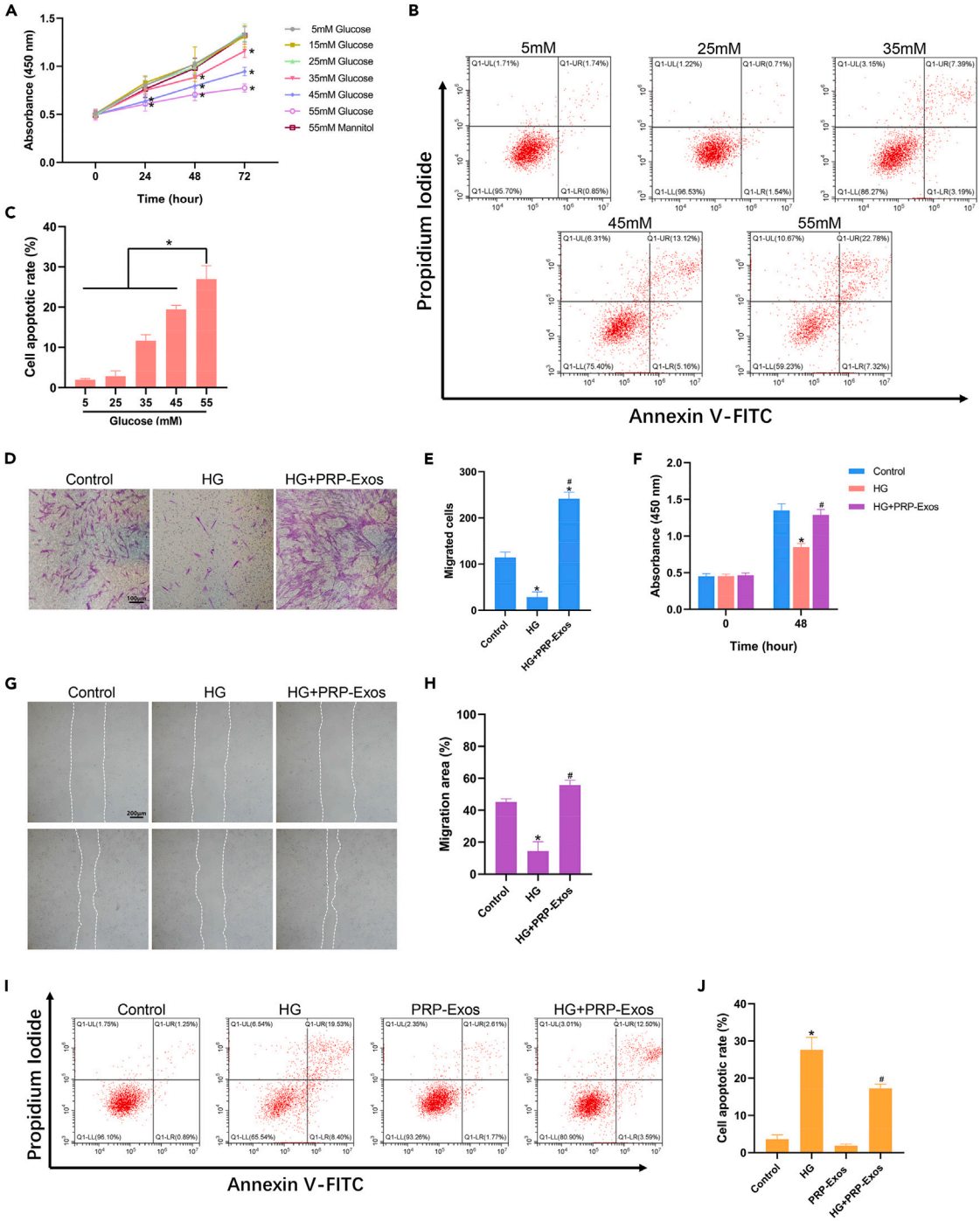

Figure 3. PRP-Exos alleviated HG-induced apoptosis and inhibition of proliferation and migration

(A) The cell viability of HSFs treated with different concentration of glucose, examined by CCK-8 analysis.

(B and C) The apoptosis of HSFs induced by different concentration of glucose, assessed through Annexin V-FITC/PI staining with flow cytometric quantitative analysis.

(D) The influence of high glucose (HG) together with or without PRP-Exos on migration of HSFs, tested by Transwell assays. Scale bar: 100 μm.

(E) Quantitative analysis of the Transwell assays.

(F) Proliferation of fibroblasts treated with HG alone or with PRP-Exos, analyzed by cck-8 assay.

(G) Migration of fibroblasts treated with HG alone or with PRP-Exos, analyzed by wound scratch assay. Scale bar: 200 μm.

(H) Quantitative analysis of the wound scratch assays.

(I) The apoptosis of HSFs induced by HG with or without PRP-Exos were assessed through Annexin V-FITC/PI double staining with flow cytometric.

(J) Quantitative analysis of cell apoptosis. *$p < 0.05$ compared with control. $^{\#}p < 0.05$ compared with HG.

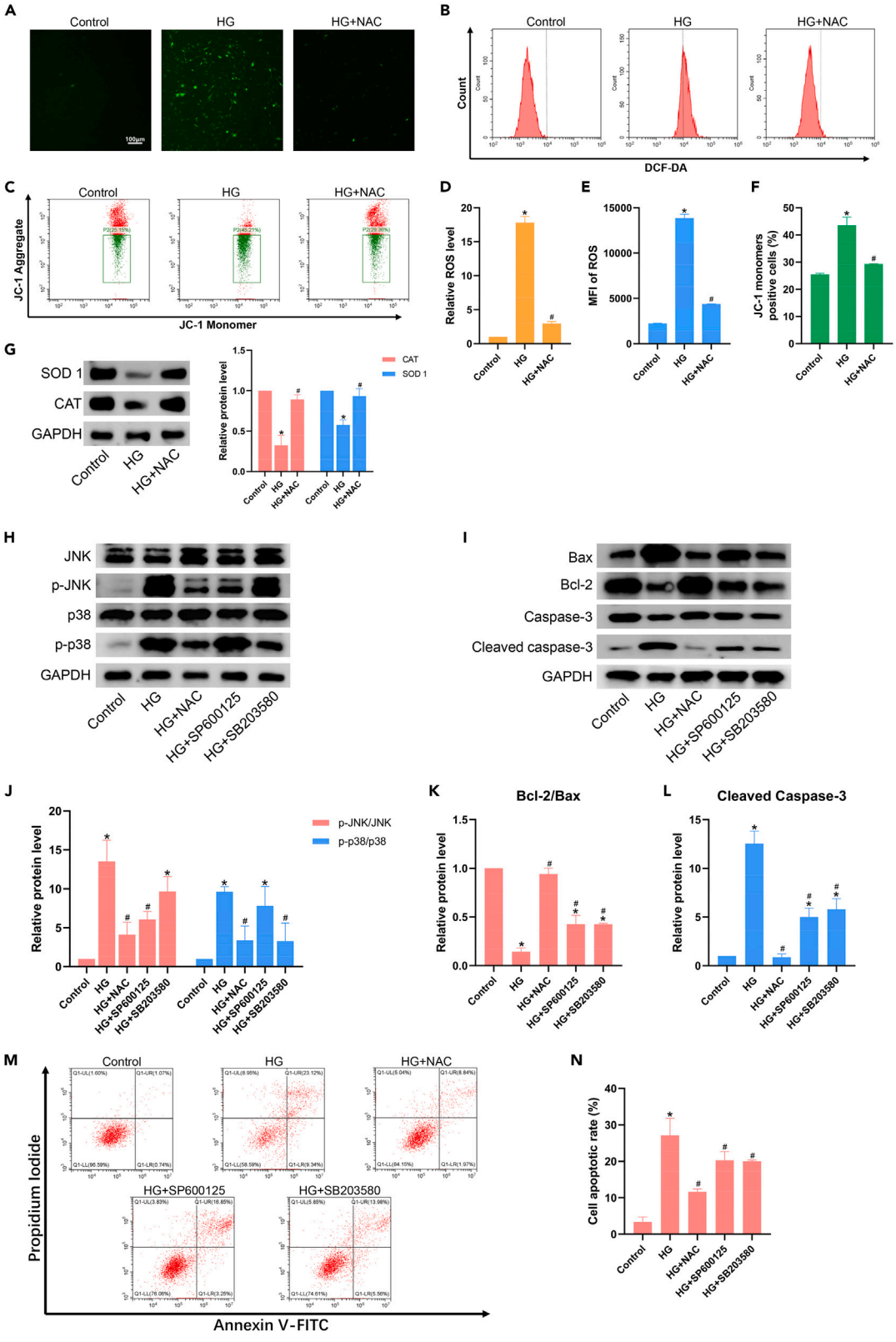
A
Control
HG
HG+NAC
100μm
B
Control
HG
HG+NAC
Count
DCF-DA
C
Control
HG
HG+NAC
JC-1 Aggregate
JC-1 Monomer
D
Relative ROS level
E
MFI of ROS
F
JC-1 monomers positive cells (%)
G
SOD 1
CAT
GAPDH
Control
HG
HG+NAC
Relative protein level
CAT
SOD 1
H
JNK
p-JNK
p38
p-p38
GAPDH
Control
HG
HG+NAC
HG+SP600125
HG+SB203580
I
Bax
Bcl-2
Caspase-3
Cleaved caspase-3
GAPDH
Control
HG
HG+NAC
HG+SP600125
HG+SB203580
J
Relative protein level
p-JNK/JNK
p-p38/p38
K
Bcl-2/Bax
Relative protein level
L
Cleaved Caspase-3
Relative protein level
M
Control
HG
HG+NAC
HG+SP600125
HG+SB203580
Propidium Iodide
Annexin V-FITC
N
Cell apoptotic rate (%)

Figure 4. HG triggered intrinsic apoptosis pathway by ROS-dependent JNK and p38 MAPK pathway

(A) Representative confocal microscope images using DCFH-DA showed that HG induced ROS production in HSFs and ROS scavenger N-acetylcysteine (NAC) significantly reduced ROS generation. Scale bar: 100 μm.

(B) ROS examined by flow cytometer using DCFH-DA.

(C) Mitochondrial membrane potential evaluated by JC-1 assay revealed that HG decreased mitochondrial membrane potential ($\Delta\Psi$m) and NAC could reverse it.

(D) Quantitative analysis of ROS generation under confocal microscope.

(E) Quantitative analysis of ROS generation measured by flow cytometer.

(F) Numerical data were expressed in terms of the ratio of JC-1 monomers positive cells.

(G) The expression of SOD 1 and CAT treated with HG with or without NAC was analyzed by western blotting. NAC reversed HG-induced inhibition of expression of SOD 1 and CAT.

(H–L) In the different treatment groups, the p-JNK, JNK, p38, p-p38, Bax, Bcl-2, caspase-3 and cleaved caspase-3 protein expression levels were examined by western blotting.

(M and N) The apoptosis of different treatment groups and quantitative analysis. *$p < 0.05$ compared with control. $^{\#}p < 0.05$ compared with HG.

These data indicate that high glucose could cause oxidative stress and trigger the mitochondrial apoptosis pathway. The JNK and p38 pathways are involved in regulating HG-induced apoptosis.

PRP-Exos rescued cells from HG-induced apoptosis without disturbing JNK and p38 MAPK pathway activation

Apoptosis of HSFs was investigated by treating the cells with PRP-Exos or HG alone or in combination. The generation of ROS with DCFH-DA probes detected by fluorescence microscopy and flow cytometry showed that PRP-Exos did not inhibit HG-induced ROS generation (Figures 5A–5D). We further examined the mitochondrial membrane potential with JC-1 probes by flow cytometry. However, the results suggested that the loss of mitochondrial membrane potential ($\Delta\Psi$m) was rescued by PRP-Exos in HSFs. The activation of Bax and Bak can lead to mitochondrial outer membrane permeabilization (MOMP) and apoptosis, and antiapoptotic Bcl-2 proteins inhibit MOMP by binding to activated Bax and Bak.[24] Hence, we continued to explore the expression of relevant proteins. The results revealed that PRP-Exos neither activate JNK and p38 nor intervene with HG-induced activation of JNK and p38. However, the downstream Bcl-2 (anti-apoptosis), Bax (pro-apoptosis), and apoptosis executive protein cleaved caspase-3 were rescued by PRP-Exos (Figures 5G–5I). These expression changes in Bcl-2 and Bax were also confirmed by PCR (Figure 5J).

The aforementioned results indicate that PRP-Exos could reverse ROS-dependent apoptosis induced by HG without disturbing JNK and p38 activation. The protective effect may be attributed to maintaining Bcl-2 expression and inhibiting Bax expression.

PRP-Exos inhibited HG-induced apoptosis through the JAK2/STAT3 pathway activated by PDGF-BB

We continued to explore the mechanism by which exosomes maintain Bcl-2 expression and inhibit Bax expression. Previously, we found that exosomes are rich in cytokines. Thus, we turned our attention to PDGF-BB, a widely investigated growth factor involved in wound healing.[25] Figure 6A shows that the expression level of PDGF receptor-β was highly increased after treatment with exosomes (Figure 6A). The JAK2/STAT3 signaling pathway is a ubiquitously expressed intracellular signaling pathway, and it participates in many vital physiological activities, including proliferation, differentiation, and apoptosis.[26] Next, the results showed that PRP-Exos could activate the JAK2/STAT3 pathway, and the application of imatinib, which is an inhibitor of PDGFRβ, significantly blocked the phosphorylation of JAK2/STAT3 (Figure 6B). This illustrates that the JAK2/STAT3 signaling pathway is activated by PDGF-BB contained in the PRP-Exos.

To investigate the role of the JAK2/STAT3 axis in alleviating apoptosis induced by HG, we applied AG490, a specific JAK2 inhibitor, and coumermycin A1, a specific JAK2 activator, to verify our hypothesis. The results of the Annexin V-FITC/PI detection assay showed that AG490 could block the anti-apoptotic effect of PRP-Exos, and the application of CA-1 in the HG environment could mimic the anti-apoptotic effect of PRP-Exos (Figures 6C and 6D). The relevant protein expression was further verified by western blotting. As shown in Figure 6E, HG did not interfere with the JAK2/STAT3 pathway. The HG+PRP-Exos group displayed marked activation by phosphorylation of JAK2/STAT3 and inhibition of Bax and cleaved caspase-3 while promoting Bcl-2. When AG490 was added to HSFs with HG and PRP-Exos, the JAK2/STAT3 axis was inhibited; therefore, the inhibition of Bax and cleaved caspase-3 was rescued, whereas Bcl-2 was inhibited. We also used CA-1 to trigger the phosphorylation of the JAK2/STAT3 axis, and the results were similar to those obtained with PRP-Exos (Figures 6E–6H).

All of these results suggest that the inhibitory effect of PRP-Exos on HG-induced apoptosis was mediated by PDGF-BB-induced activation of the JAK2/STAT3 pathway.

Combined application of PRP-Exos and HP-PEG/HA-SH hydrogel promoted diabetic wound healing in diabetic rats model

Cytotoxicity of hydrogels

To evaluate the cytotoxicity of the hydrogels, we used CCK-8 assays to examine the cell viability in Transwell 96-well plates. After coculture of HSFs and hydrogel for 24 or 48 h, the OD value detected by CCK-8 showed no difference, which indicates that HP-PEG/HA-SH hydrogels are nontoxic to HSFs (Figure 7A).

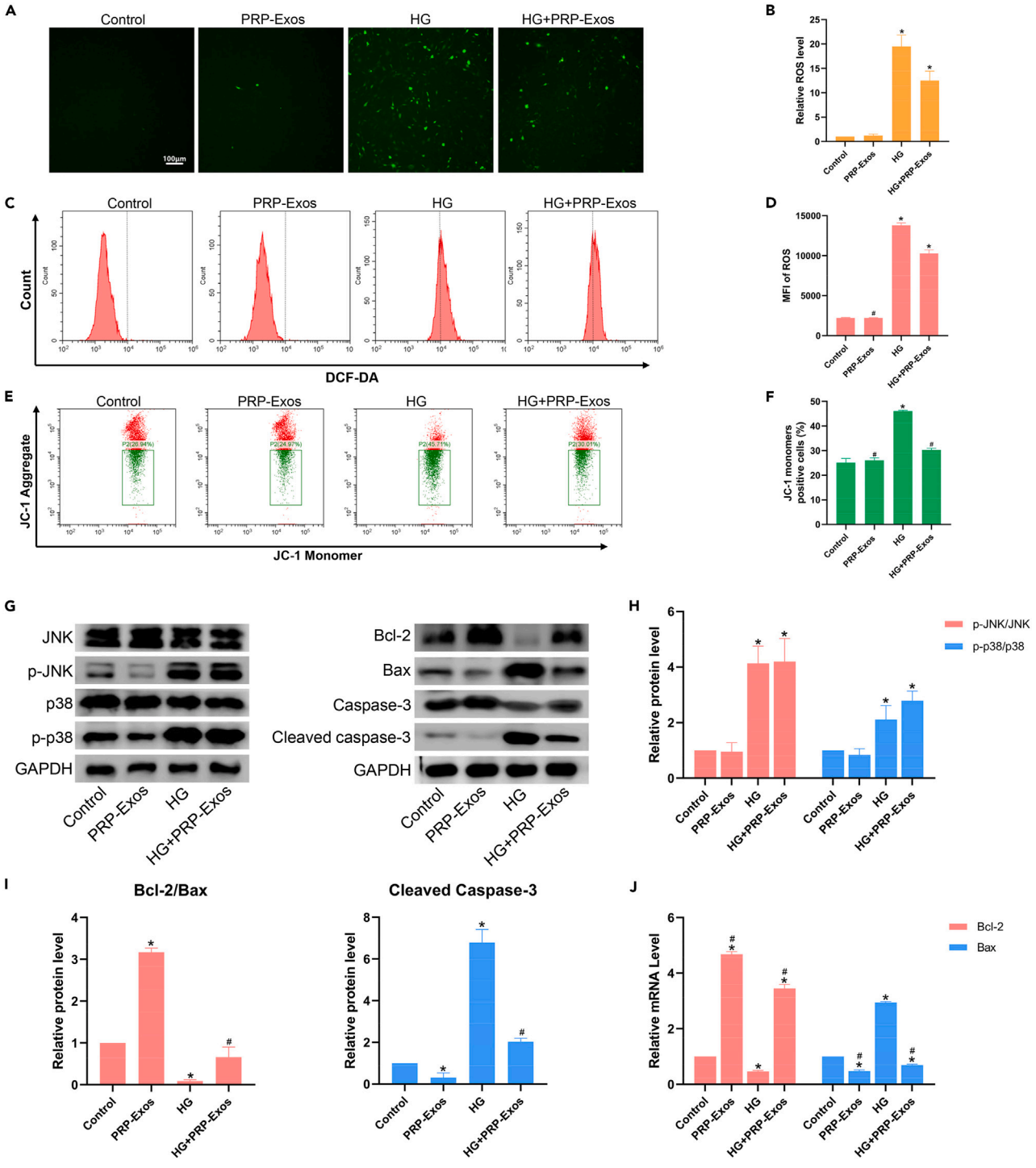

Figure 5. PRP-Exos rescued cells from HG-induced apoptosis without disturbing JNK and p38 MAPK pathway activation

(A) Representative confocal microscope images using DCFH-DA in groups treated with HG, PRP-Exos or both.

(B) Quantitative analysis of ROS measured by confocal microscope using DCFH-DA. Scale bar: 100 μm.

(C) Quantification of ROS generation tested by flow cytometer in all groups.

(D) Quantification analysis of the fluorescent intensity.

(E) Changes of mitochondrial membrane potential ($\Delta\Psi m$) were analyzed by JC-1 and measured by flow cytometer.

(F) Quantification analysis of the ratio of JC-1 monomers positive cells.

(G–J) The expression levels of JNK, p-JNK, p38, p-p38, Bax, Bcl-2, caspase-3, and cleaved caspase-3 investigated by western blotting in different groups. *$p < 0.05$ compared with control. #$p < 0.05$ compared with HG.

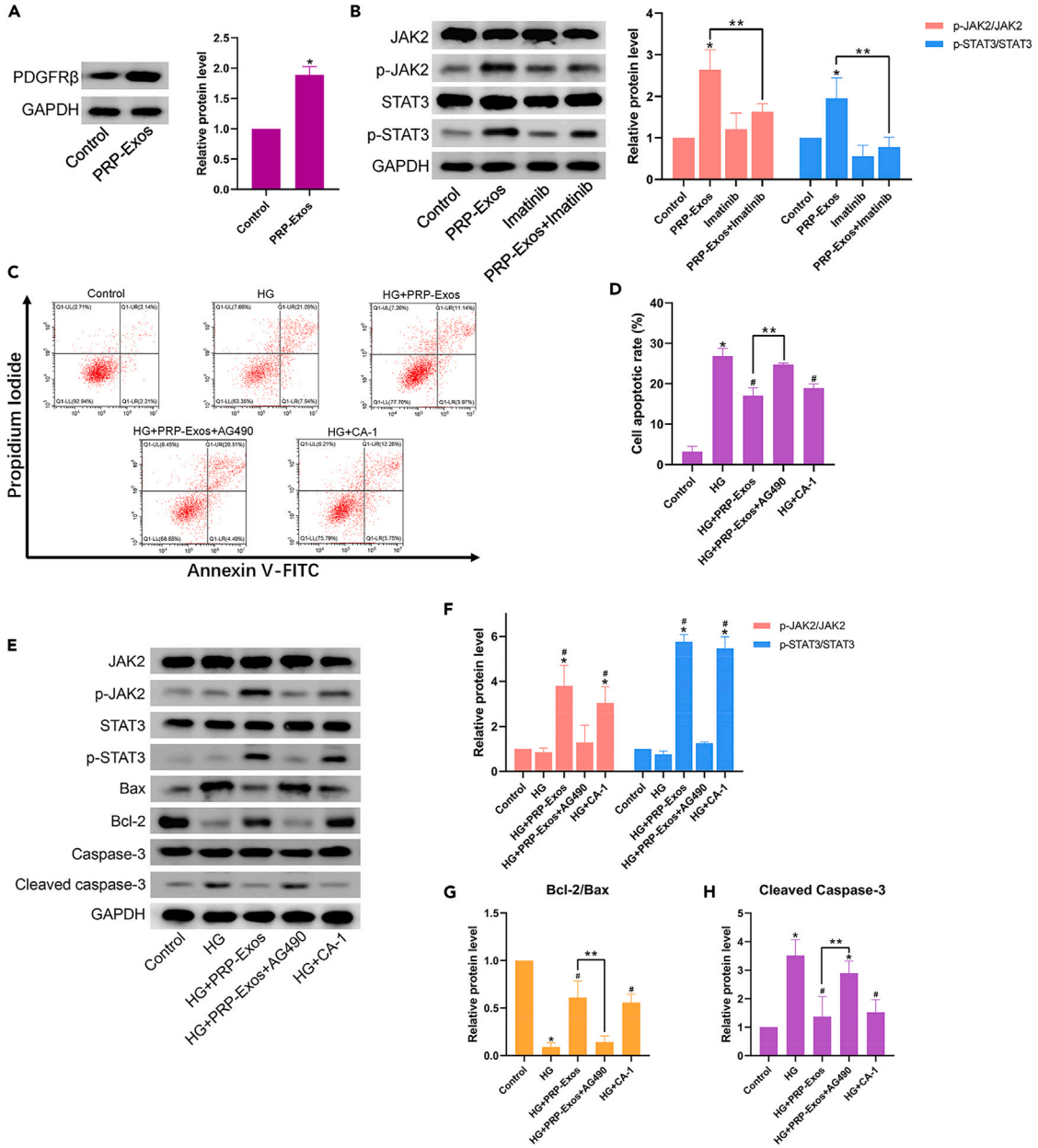

Figure 6. PRP-Exos inhibited HG-induced apoptosis through JAK2/STAT3 pathway activated by PDGF-BB

(A) The expression level of PDGFRβ detected by western blotting, PRP-Exos significantly increased the expression level of PDGFRβ.

(B) JAK2 and STAT3 phosphorylation level in fibroblasts treated with PRP-Exos together with or without imatinib. Imatinib blocked the activation of JAK2 and STAT3 induced by PRP-Exos.

(C and D) The apoptosis induced by HG together with specific treatment was assessed through Annexin V-FITC/PI double staining with flow cytometric analysis.

(E–H) The expression levels of JAK2, p-JAK2, STAT3, p-STAT3, Bax, Bcl-2, caspase-3 and cleaved caspase-3 in groups that received different treatments were examined by western blotting. *p < 0.05 compared with control. #p < 0.05 compared with HG. **p < 0.05 compared between specific groups.

Release of PRP-Exos from hydrogels

The sustained release ability of HP-PEG/HA-SH hydrogels was tested by a BCA protein quantification kit at 12, 24, 48, 72, and 96 h. We found that the protein was present in the solution around the hydrogel, indicating leaching (Figure 7B). This indicates that the PRP-Exos embedded in HP-PEG/HA-SH hydrogels can be sustained and released for at least 96 h.

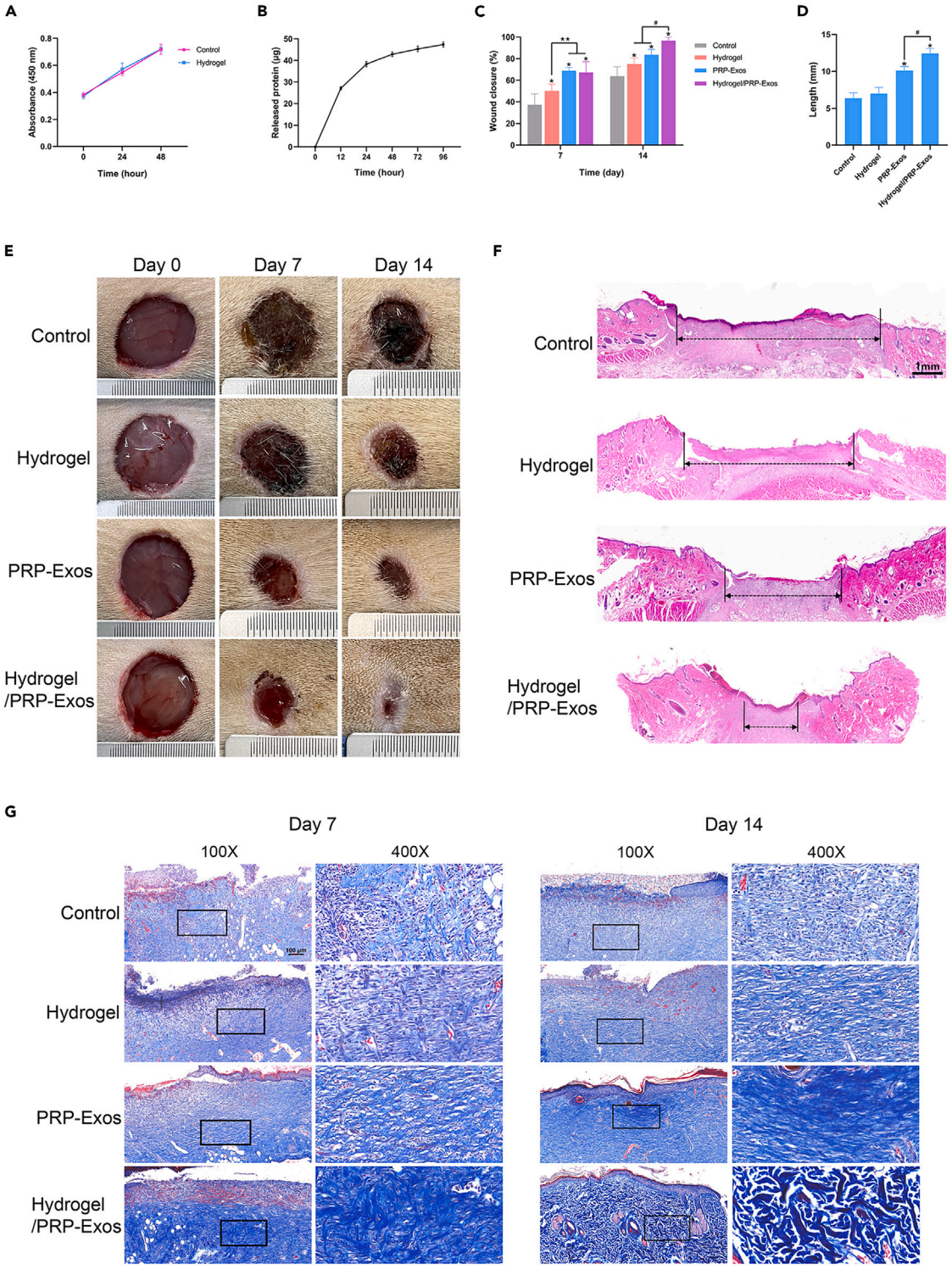

Figure 7. The promoting effects of PRP-Exos on wound healing in diabetic rat model

(A) Cytotoxicity of the HP-PEG/HA-SH hydrogel was analyzed by CCK-8 assay, the OD value was measured at 0, 24, and 48 h.

(B) The sustained release ability of HP-PEG/HA-SH hydrogels was tested by BCA protein quantification kit at 12, 24, 48, 72, and 96 h; cumulative amount of released protein was represented.

(C) Quantitative analysis of wound closure percentage at 7and 14 days.

(D) Quantitative analysis of the extent of re-epithelialization at 14 days (Length = original wound length−wound length at 14 days).

Figure 7. *Continued*

(E) Representative images of full-thickness excisional wound in a diabetic rat model; four groups were involved: control, hydrogel, PRP-Exos, and hydrogel/PRP-Exos. Images were recorded at 0, 7, and 14 days after operation.

(F) H&E staining of wound sections received different treatments at 14 days after operation. The black arrows indicate the re-epithelialization. Scale bar: 1 mm.

(G) Masson's trichrome-stained wound sections of different groups at 7 and 14 days after operation, indicating collagen deposition. Scale bar: 100 μm. *$p < 0.05$ compared with control. $^{\#}p < 0.05$ and **$p < 0.05$ compared between specific groups.

PRP-Exos promote the diabetic wound healing process

Humanized full-thickness excisional wound models were developed in STZ-induced diabetic SD rats to test PRP-Exo efficacy *in vivo*.[27] Four treatment groups were set: control (no treatment), hydrogel (100 μL gel without exosomes), PRP-Exos (200 μg exosomes, subcutaneous injection), and hydrogel/PRP-Exos (100 μL gel containing 200 μg exosomes). Digital photographs were taken during the process of healing of all groups at 0, 7, and 14 days, and the groups with specific treatments showed better healing. In particular, wounds in the hydrogel/PRP-Exos group were almost entirely healed at Day 14 (Figure 7E). In terms of wound closure, the PRP-Exos and hydrogel/PRP-Exos groups did not differ significantly at 7 days, but at 14 days, the hydrogel/PRP-Exos group revealed the best capacity for promoting wound healing (Figure 7C).

Histologic analyses

For histologic analysis, the wound samples were stained with HE to evaluate the neoepithelium at 14 days (Figure 7F). The initial wound size was the same (1.5 cm). The hydrogel/PRP-Exos treatment groups showed significantly better epithelia than the other groups, whereas the PRP-Exos treatment groups showed better epithelia than the hydrogel treatment groups. Meanwhile, the groups that received treatment had better results than the control group (Figure 7D). Collagen was evaluated by Masson's trichrome staining. The PRP-Exos group and hydrogel/PRP-Exos group showed a greater extent of collagen deposition and large wavy collagen fibers compared with the hydrogel group and control group at 7 and 14 days. Interestingly, the hydrogel/PRP-Exos group showed higher collagen fiber levels and a well-organized matrix than the other groups at 14 days (Figure 7G). The aforementioned results confirm the dramatic enhancement of collagen remodeling and epithelial regeneration through PRP-Exos.

Immunohistochemistry and immunofluorescence analysis

IHC and IF staining were applied to detect the influence of PRP-Exos on angiogenesis at Day 14. CD31 is located on the surface of endothelial cells, and α-SMA is localized on smooth muscle cells; both are known markers for vascular networks. The number of CD31- and α-SMA-positive vessels in each wound was counted in IHC analysis to reflect the newly formed blood vessels (Figure 8A). Quantification of the new blood vessels showed that the PRP-Exos group and hydrogel/PRP-Exos group had significantly enhanced angiogenesis and that the hydrogel/PRP-Exos group exhibited a stronger angiogenesis function than the PRP-Exos group. Furthermore, CD31 and α-SMA costaining indicated mature vessels in the IF analysis (Figure 8D). Quantification of the mature blood vessels revealed that the generation level of mature vessels in the hydrogel/PRP-Exos group was the highest at 14 days. These results also validated that the sustained release ability of HP-PEG/HA-SH hydrogels amplifies the function of PRP-Exos.

DISCUSSION

Researchers and clinicians are increasingly interested in applying PRP for tissue engineering.[28] PRP is a concentrated platelet product derived from whole blood that is widely used in regenerative medicine and has already proven effective in clinical practice. Upon activation, the platelets immediately degranulate, releasing multiple GFs.[29,30] Furthermore, extracellular vesicles (EVs), vital paracrine mediators released by cells, such as exosomes and microvesicles, may contribute to cell-to-cell communication.[12,31] PRP's effects are thought to be mediated in part through efficient intercellular communication of bioactive molecules by nanosized vesicles called exosomes.[15] Exosomes isolated from PRP have curative potential in tissue repair, osteoarthritis, osteonecrosis, and muscle injury.[16–20] However, two of the studies on diabetic wound healing did not involve the study of the mechanism of delayed wound healing caused by diabetes and failed to systematically confirm the protective effect of PRP-Exos on fibroblasts in diabetic environments both *in vitro* and *in vivo*.[16,20] GFs have also been found in exosomes from PRP, and they are very effective for wound healing.[16] In relation to wound repair, PDGFBB, VEGF, and bFGF are the most strongly associated growth factors secreted by PRP,[31] as they are involved in regeneration and possibly regulate HMEC-1 cells and fibroblasts.[32] In our study, exosomes were successfully extracted from PRP and identified, and GFs related to wound repair, such as PDGFBB, VEGF, and bFGF, were encapsulated within these exosomes, suggesting that growth factors are delivered across the extracellular space by PRP-Exos, facilitating tissue regeneration. The PRP-Exos were validated to promote proliferation and migration of HSFs in our study *in vitro* and *in vivo*. In addition, CD41 was used as a source marker of platelets because platelets are generally degranulated from megakaryocytes that highly express CD41.

Healing occurs as a result of hemostasis, inflammation, proliferation, epithelialization, and remodeling.[25] The repair process will begin with hemostasis, and platelets are activated at this stage, leading to platelet aggregation, clotting, and factor release, resulting in fibrin clot generation at the wound site. Meanwhile, inflammatory cells are recruited to clean up the debris and pathogens and prepare the environment for the next step, and during the late inflammatory phase, fibroblasts start to come into play.[33] Soft tissue wound healing relies on fibroblasts to contract wounds, synthesize collagen, and remodel tissues. The proliferation and migration of fibroblasts are crucial for wound healing.[2,3]

Diabetes, as a multifaceted metabolic disease, is increasingly prevalent worldwide and places a serious burden on patients and healthcare systems.[34] Chronic wounds induced by DM have received increasing attention but still lack effective therapeutic interventions. Diabetic wounds have an exceptionally complex pathology, and hyperglycemia-induced oxidative stress is believed to be one major causative factor.[5]

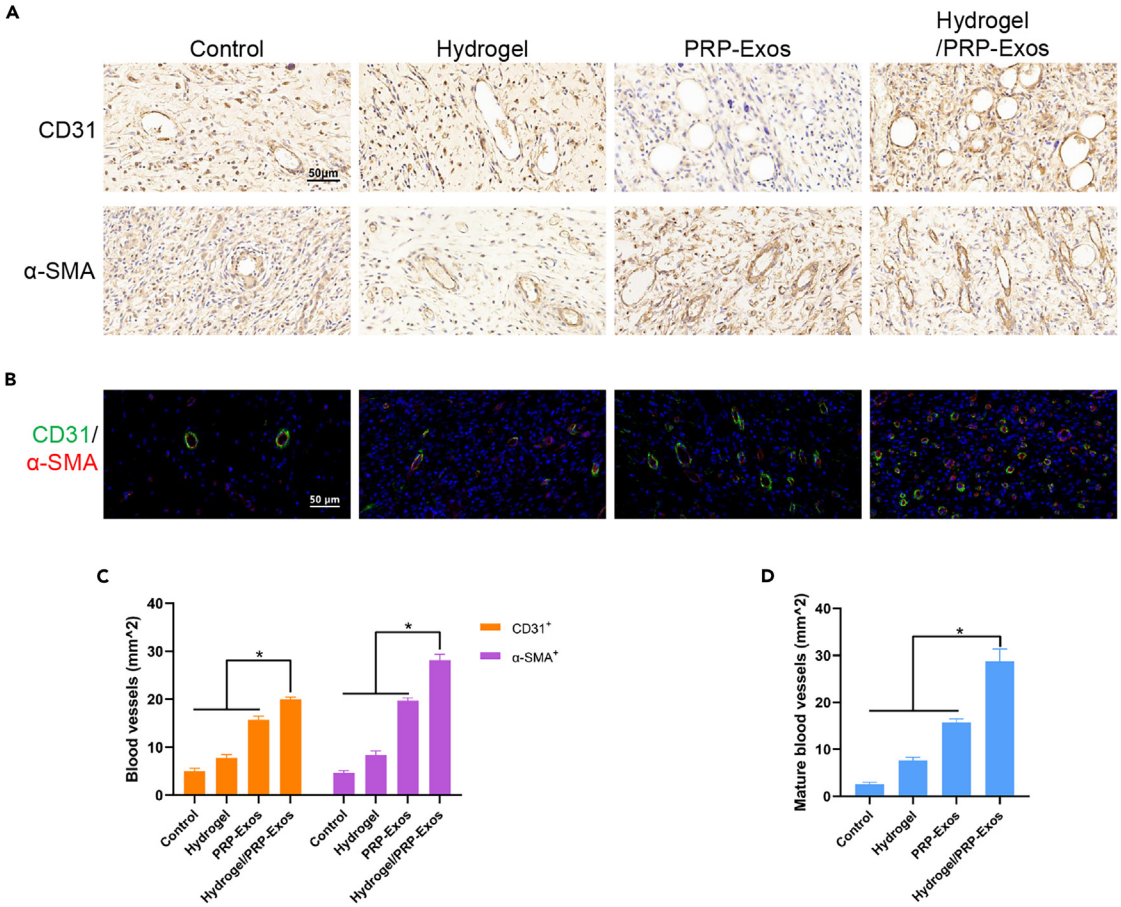

Figure 8. The promotion effects of PRP-Exos on angiogenesis

(A) IHC staining of CD31 and α-SMA at 14 days. Newly formed blood vessels were identified by positive CD31 or positive α-SMA staining and their typical oval structures. Scale bar: 50 μm.

(B) IF staining of CD31 and α-SMA at 14 days. CD31 and α-SMA are stained green and red, respectively. Red and green co-staining stands for mature blood vessels. Scale bar: 50 μm.

(C) Quantitative analysis of newly formed blood vessels based on CD31- and a-SMA-positive stained vasculature.

(D) Quantitative analysis of mature blood vessels. CD31 is located on the surface of endothelial cells; α-SMA is localized on smooth muscle cells. *p < 0.05 compared between specific groups.

Hyperglycemia can upregulate oxidative stress through different metabolic pathways, such as glycolytic, hexosamine, protein kinase C, polyol, and advanced glycation end product (AGE) pathways.[22] Nonhealing diabetic wounds exhibit a highly oxidizing environment, and this impairs fibroblasts in their regeneration process.[4] Therefore, our study used high glucose to mimic abnormal hyperglycemia in HSFs *in vitro*, and the results suggested that HG significantly blocked proliferation and migration and induced apoptosis. As expected, after the addition of PRP-Exos, the cell apoptosis and impaired biological behavior were reversed.

Apoptosis, an essential and widely investigated type of programmed cell death, is involved in many physiological activities, such as metabolism, development, and immune homeostasis.[35] As discussed widely, mitochondria are a crucial part of the initiation of intrinsic apoptosis, one of the two main apoptotic signaling pathways.[36] Diverse cellular stresses, including deprivation of growth factors, DNA damage, or oxidative stress, could lead to apoptosis via the intrinsic or mitochondrial pathway. When the intrinsic pathway is activated, proapoptotic proteins are released from the intermembrane space of the mitochondria as a result of mitochondrial outer membrane permeabilization (MOMP).[21] In our work, we found that HG induced ROS overproduction and apoptosis. Therefore, we investigated the specific mechanism underlying the apoptosis and whether PRP-Exos could intervene. Researchers have shown that MAPK pathways are involved in many cellular activities, including development, proliferation, differentiation, and apoptosis, in response to extracellular stimuli. Among them, JNK and p38 MAPK are activated most notably when cells are exposed to physical, chemical, and biological stress.[37,38] The data suggested that HG induced oxidative stress and JNK and p38 MAPK activation. When the ROS scavenger NAC was added, the ROS level decreased to normal levels, JNK and p38 MAPK were inactivated, and the HG-induced apoptotic effect was totally blocked. Likewise, the use of SP600125, a specific JNK inhibitor, and SB203580, a p38 inhibitor, partly blocked apoptosis, whereas the ROS level was not disturbed. This finding indicates that HG-induced apoptosis occurs through ROS-dependent activation of the JNK and p38 MAPK pathways.

Furthermore, we examined how PRP-Exos attenuate HG-induced apoptosis. The ROS level results revealed that PRP-Exos neither induced ROS production nor affected HG-induced ROS production. However, the JC-1 results showed that PRP-Exos could preserve the mitochondrial membrane potential, which is based on the protein expression ratio of Bcl-2 and Bax. These results were confirmed by western blotting: PRP-Exos did not affect the HG-induced activation of JNK or p38 but maintained the Bcl-2 levels and inhibited the upregulation of Bax. Both Bax and Bcl-2 belong to the Bcl-2 protein family.[39] Activated Bax and Bak can cause MOMP and apoptosis, whereas Bcl-2 proteins have the ability to bind activated Bax and Bak effectors and prevent MOMP.[24] This finding suggests that the anti-apoptotic effect of PRP-Exos is due to other pathways.

It has been widely demonstrated that the bioactive promoting influence of PRP is due to diverse growth factors, and these GFs were also found in PRP-Exos in our study. Thus, we turned our attention toward the GFs enriched in the PRP-Exos. PDGF-BB, a growth factor derived from platelets, has been recognized as a potent growth factor for fibroblasts since its discovery in platelets.[40–42] Multiple signaling pathways can be activated by PDGF-BB binding to the two extracellular domains of receptors, PDGFRα and PDGFRβ. Their promotion effects on fibroblasts are most predominantly mediated through PDGFRβ.[32,43] Therefore, we studied the role of PDGF-BB encapsulated in PRP-Exos. First, we tested the protein expression of PDGFRβ, and the results suggested that after the addition of PRP-Exos, the PDGFRβ expression level markedly improved. This result indicated that PRP-Exos indeed activated PDGFRβ. The JAK/STAT signaling pathway regulates multiple body functions, such as cell proliferation, differentiation, apoptosis, immune function, and hematopoiesis.[44] Several studies have confirmed that PDGF-BB can promote fibroblast proliferation and differentiation through the JAK2/STAT3 signaling pathway.[42,45] Accordingly, we were curious about whether the JAK2/STAT3 pathway could be activated by PDGF-BB. Our data revealed that PRP-Exos activate the JAK2/STAT3 pathway and imatinib, an inhibitor preventing PDGFRβ autophosphorylation upon PDGF-BB binding, blocks the activation effect of PRP-Exos on the JAK2/STAT3 axis.

To this point, our data indicated that PDGF-BB in PRP-Exos activated the JAK2/STAT3 pathway. Previously, we discovered that the inhibitory apoptosis effect of PRP-Exos is ascribed to the maintenance of Bcl-2 and the inhibition of Bax. As a classic prosurvival signaling axis, the JAK2/STAT3 pathway possesses the capacity to promote Bcl-2, inhibit Bax, and subsequently relieve apoptosis. Therefore, we next investigated whether the anti-apoptotic effect of PRP-Exos involved the JAK2/STAT3 pathway. AG490 and CA-1 were used to inhibit or activate the JAK2/STAT3 pathway, respectively. After treatment, AG490 significantly attenuated the anti-apoptotic effect of PRP-Exos, and CA-1 enhanced the anti-apoptotic effect as shown by the Annexin V-FITC/PI assay. Protein expression was further analyzed by western blotting, and HG decreased the level of Bcl-2/Bax without affecting the JAK2/STAT3 pathway. PRP-Exos successfully activated the JAK2/STAT3 pathway and promoted the level of Bcl-2/Bax, as expected. Moreover, after AG490 blocked the JAK2/STAT3 axis, the Bcl-2/Bax level decreased to a level similar to that in the HG group. When CA-1 was added under conditions of high glucose, JAK2/STAT3 was phosphorylated, and the Bcl-2/Bax level was improved. The expression trends of the apoptosis effector protein cleaved caspase-3 were the same as those of the proapoptotic protein Bax. The results demonstrated that PRP-Exos alleviated HG-induced HSF apoptosis by maintaining the Bcl-2/Bax level through PDGF-BB-induced activation of the JAK2/STAT3 pathway.

The recent development of hydrogel systems for wound healing has received much attention.[46–48] Hydrogels can be injected and applied to any irregular condition, and they possess many advantages, such as maintaining cell activity, minimal invasion, and a sustained release ability.[46] Based on these advantages, we chose an injectable HP-PEG/HA-SH hydrogel as an exosome-delivery platform to validate the promoting ability of PRP-Exos *in vivo*. We confirmed the biocompatibility and sustained-release ability of the hydrogel *in vitro*. The comparison between the hydrogel/PRP-Exos group and the PRP-Exos group showed that the hydrogel could improve the biological effects of PRP-Exos. The results between the hydrogel/PRP-Exos group and the hydrogel group eliminated the interference from hydrogels on results and successfully proved the promoting ability of PRP-Exos. Finally, our results found that the application of PRP-Exos alone showed a significant effect of promoting wound healing, while the application of hydrogel alone also had a promotion effect, and the promotion effect was the strongest when the two were applied in combination. Therefore, we inferred that PRP-Exos have the potential to promote diabetic wound healing, and the hydrogel can enhance the promoting effect of PRP-Exos in accelerating diabetic wound healing and angiogenesis.

In summary, our results confirmed the capacity of PRP-Exos to promote diabetic wound healing both *in vitro* and *in vivo* for the first time. Our study found that the PDGF-BB-induced JAK2/STAT3 signaling pathway plays a vital role in the protective effect of PRP-Exos on apoptosis resulting from oxidative stress. This study will help elucidate the mechanism by which PRP-Exos promote wound healing. Of course, there are still many limitations of this study. First, high glucose could not simulate the diabetic environment entirely due to its complex pathogenic mechanisms. Second, other growth factors in PPR-Exos may also be involved, and this needs further investigation.

In summary, our work demonstrates for the first time that PRP-Exos protect fibroblasts from HG environment *in vitro* and promote diabetic wound healing *in vivo*. In HSFs, high glucose induces oxidative stress and activates the JNK and p38 pathways to inhibit cell proliferation and survival. PRP-Exos rescue the negative influence of HG without disturbing HG-induced oxidative stress or the JNK and p38 signaling pathways. Under HG-induced oxidative stress, PRP-Exos block the ROS/JNK and p38-mediated inhibition of Bcl-2 protein expression and promote Bax protein expression via the JAK2/STAT3/Bcl-2 pathway, saving the cell from apoptosis.

Limitations of the study

PRP-Exos contain a variety of growth factors. Our study only focused on the protective effect of PDGF-BB on fibroblasts. The biological effects of other growth factors need further exploration. The wound healing process is complex and involves many kinds of cells. The interaction between other cells, such as vascular endothelial cells and inflammatory cells, and PRP-Exos also deserves further study. Moreover, SEM microstructure (structure and exosome integrity) of hydrogel/PRP-Exos composites still need to be further verified in future research.

STAR★METHODS

Detailed methods are provided in the online version of this paper and include the following:

- KEY RESOURCES TABLE
- RESOURCE AVAILABILITY
  - Lead contact
  - Materials availability
  - Data and code availability
- EXPERIMENTAL MODEL AND STUDY PARTICIPANT DETAILS
  - Cell culture studies
  - Animals
- METHOD DETAILS
  - Platelet-rich plasma (PRP) extraction
  - PRP-derived exosome (PRP-Exo) extraction
  - Identification of PRP-Exos
  - Hydrogel and PRP-Exos-loaded hydrogel preparation
  - Exosome uptake by HSFs
  - Cell proliferation assay
  - Cell migration assay
  - Cell apoptosis assay
  - ROS measurement
  - Mitochondrial membrane potential detection
  - Western Blot
  - qRT−PCR analysis
  - Cytotoxicity assays
  - Release profile of PRP-Exos-loaded hydrogel
  - Histological analysis
  - Immunohistochemistry and immunofluorescence analysis
- QUANTIFICATION AND STATISTICAL ANALYSIS

ACKNOWLEDGMENTS

This work was supported by the Guide Project for Key Research and Development Foundation of Liaoning Province (No. 2019JH8/10300018 and 2018225122) and the Science and Technology Planning Project in Shenyang (22-321-32-12).

AUTHOR CONTRIBUTIONS

W.C.: Data curation, Methodology, Formal analysis, Writing—original draft; X.M.: Data curation, Formal analysis, Methodology, Investigation.; F.C.: Data curation, Investigation, Software, Formal analysis; J.W.: Conceptualization, Software, Validation; M.Y.: Funding acquisition, Project administration, Resources, Writing—review and editing. All authors read and approved the manuscript.

DECLARATION OF INTERESTS

The authors declare no competing interests.

Received: August 4, 2023
Revised: August 26, 2023
Accepted: October 13, 2023
Published: October 17, 2023

REFERENCES

1. Burgess, J.L., Wyant, W.A., Abdo Abujamra, B., Kirsner, R.S., and Jozic, I. (2021). Diabetic Wound-Healing Science. Medicina *57*, 1072. https://doi.org/10.3390/medicina57101072.
2. Driskell, R.R., Lichtenberger, B.M., Hoste, E., Kretzschmar, K., Simons, B.D., Charalambous, M., Ferron, S.R., Herault, Y., Pavlovic, G., Ferguson-Smith, A.C., and Watt, F.M. (2013). Distinct fibroblast lineages determine dermal architecture in skin development and repair. Nature *504*, 277–281. https://doi.org/10.1038/nature12783.
3. Bainbridge, P. (2013). Wound healing and the role of fibroblasts. J. Wound Care *22*, 407-8–410-12. https://doi.org/10.12968/jowc.2013.22.8.407.
4. Wan, R., Weissman, J.P., Grundman, K., Lang, L., Grybowski, D.J., and Galiano, R.D. (2021). Diabetic wound healing: The impact of diabetes on myofibroblast activity and its potential therapeutic treatments. Wound Repair Regen. *29*, 573–581. https://doi.org/10.1111/wrr.12954.
5. Ighodaro, O.M. (2018). Molecular pathways associated with oxidative stress in diabetes mellitus. Biomed. Pharmacother. *108*, 656–662. https://doi.org/10.1016/j.biopha.2018.09.058.

6. Deng, L., Du, C., Song, P., Chen, T., Rui, S., Armstrong, D.G., and Deng, W. (2021). The Role of Oxidative Stress and Antioxidants in Diabetic Wound Healing. Oxid. Med. Cell. Longev. *2021*, 8852759. https://doi.org/10.1155/2021/8852759.
7. Chicharro-Alcántara, D., Rubio-Zaragoza, M., Damiá-Giménez, E., Carrillo-Poveda, J.M., Cuervo-Serrato, B., Peláez-Gorrea, P., and Sopena-Juncosa, J.J. (2018). Platelet Rich Plasma: New Insights for Cutaneous Wound Healing Management. J. Funct. Biomater. *9*, 10. https://doi.org/10.3390/jfb9010010.
8. Dhillon, R.S., Schwarz, E.M., and Maloney, M.D. (2012). Platelet-rich plasma therapy - future or trend? Arthritis Res. Ther. *14*, 219. https://doi.org/10.1186/ar3914.
9. Grigore, T.V., and Cozma, C. (2018). Platelet-rich plasma as a site-targeted approach in wound healing: a molecular perspective. Discoveries *6*, e87. https://doi.org/10.15190/d.2018.8.
10. Wu, J., Piao, Y., Liu, Q., and Yang, X. (2021). Platelet-rich plasma-derived extracellular vesicles: A superior alternative in regenerative medicine? Cell Prolif. *54*, e13123. https://doi.org/10.1111/cpr.13123.
11. Chahla, J., Cinque, M.E., Piuzzi, N.S., Mannava, S., Geeslin, A.G., Murray, I.R., Dornan, G.J., Muschler, G.F., and LaPrade, R.F. (2017). A Call for Standardization in Platelet-Rich Plasma Preparation Protocols and Composition Reporting: A Systematic Review of the Clinical Orthopaedic Literature. J. Bone Joint Surg. Am. *99*, 1769–1779. https://doi.org/10.2106/JBJS.16.01374.
12. Tkach, M., and Théry, C. (2016). Communication by Extracellular Vesicles: Where We Are and Where We Need to Go. Cell *164*, 1226–1232. https://doi.org/10.1016/j.cell.2016.01.043.
13. Robbins, P.D., and Morelli, A.E. (2014). Regulation of immune responses by extracellular vesicles. Nat. Rev. Immunol. *14*, 195–208. https://doi.org/10.1038/nri3622.
14. Burgess, D.J. (2014). Signalling: vesicle vehicles of genetic information. Nat. Rev. Genet. *15*, 514. https://doi.org/10.1038/nrg3780.
15. Torreggiani, E., Perut, F., Roncuzzi, L., Zini, N., Baglìo, S.R., and Baldini, N. (2014). Exosomes: novel effectors of human platelet lysate activity. Eur. Cell. Mater. *28*, 137–151. , discussion 151. https://doi.org/10.22203/ecm.v028a11.
16. Guo, S.C., Tao, S.C., Yin, W.J., Qi, X., Yuan, T., and Zhang, C.Q. (2017). Exosomes derived from platelet-rich plasma promote the re-epithelization of chronic cutaneous wounds via activation of YAP in a diabetic rat model. Theranostics *7*, 81–96. https://doi.org/10.7150/thno.16803.
17. Tao, S.C., Yuan, T., Rui, B.Y., Zhu, Z.Z., Guo, S.C., and Zhang, C.Q. (2017). Exosomes derived from human platelet-rich plasma prevent apoptosis induced by glucocorticoid-associated endoplasmic reticulum stress in rat osteonecrosis of the femoral head via the Akt/Bad/Bcl-2 signal pathway. Theranostics *7*, 733–750. https://doi.org/10.7150/thno.17450.
18. Iyer, S.R., Scheiber, A.L., Yarowsky, P., Henn, R.F., Otsuru, S., and Lovering, R.M. (2020). Exosomes Isolated From Platelet-Rich Plasma and Mesenchymal Stem Cells Promote Recovery of Function After Muscle Injury. Am. J. Sports Med. *48*, 2277–2286. https://doi.org/10.1177/0363546520926462.
19. Zhang, Y., Wang, X., Chen, J., Qian, D., Gao, P., Qin, T., Jiang, T., Yi, J., Xu, T., Huang, Y., et al. (2022). Exosomes derived from platelet-rich plasma administration in site mediate cartilage protection in subtalar osteoarthritis. J. Nanobiotechnol. *20*, 56. https://doi.org/10.1186/s12951-022-01245-8.
20. Chen, C., Wang, Q., Li, D., Qi, Z., Chen, Y., and Wang, S. (2023). MALAT1 participates in the role of platelet-rich plasma exosomes in promoting wound healing of diabetic foot ulcer. Int. J. Biol. Macromol. *238*, 124170. https://doi.org/10.1016/j.ijbiomac.2023.124170.
21. Bock, F.J., and Tait, S.W.G. (2020). Mitochondria as multifaceted regulators of cell death. Nat. Rev. Mol. Cell Biol. *21*, 85–100. https://doi.org/10.1038/s41580-019-0173-8.
22. Giacco, F., and Brownlee, M. (2010). Oxidative stress and diabetic complications. Circ. Res. *107*, 1058–1070. https://doi.org/10.1161/CIRCRESAHA.110.223545.
23. Sui, X., Kong, N., Ye, L., Han, W., Zhou, J., Zhang, Q., He, C., and Pan, H. (2014). p38 and JNK MAPK pathways control the balance of apoptosis and autophagy in response to chemotherapeutic agents. Cancer Lett. *344*, 174–179. https://doi.org/10.1016/j.canlet.2013.11.019.
24. Llambi, F., Moldoveanu, T., Tait, S.W.G., Bouchier-Hayes, L., Temirov, J., McCormick, L.L., Dillon, C.P., and Green, D.R. (2011). A unified model of mammalian BCL-2 protein family interactions at the mitochondria. Mol. Cell *44*, 517–531. https://doi.org/10.1016/j.molcel.2011.10.001.
25. Gurtner, G.C., Werner, S., Barrandon, Y., and Longaker, M.T. (2008). Wound repair and regeneration. Nature *453*, 314–321. https://doi.org/10.1038/nature07039.
26. O'Shea, J.J., Schwartz, D.M., Villarino, A.V., Gadina, M., McInnes, I.B., and Laurence, A. (2015). The JAK-STAT pathway: impact on human disease and therapeutic intervention. Annu. Rev. Med. *66*, 311–328. https://doi.org/10.1146/annurev-med-051113-024537.
27. Wong, V.W., Sorkin, M., Glotzbach, J.P., Longaker, M.T., and Gurtner, G.C. (2011). Surgical approaches to create murine models of human wound healing. J. Biomed. Biotechnol. *2011*, 969618. https://doi.org/10.1155/2011/969618.
28. Etulain, J. (2018). Platelets in wound healing and regenerative medicine. Platelets *29*, 556–568. https://doi.org/10.1080/09537104.2018.1430357.
29. Martinez-Zapata, M.J., Marti-Carvajal, A.J., Sola, I., Exposito, J.A., Bolibar, I., Rodriguez, L., Garcia, J., and Zaror, C. (2016). Autologous platelet-rich plasma for treating chronic wounds. Cochrane Database Syst. Rev. CD006899. https://doi.org/10.1002/14651858.CD006899.pub3.
30. Hesseler, M.J., and Shyam, N. (2019). Platelet-rich plasma and its utility in medical dermatology: A systematic review. J. Am. Acad. Dermatol. *81*, 834–846. https://doi.org/10.1016/j.jaad.2019.04.037.
31. Cabral, J., Ryan, A.E., Griffin, M.D., and Ritter, T. (2018). Extracellular vesicles as modulators of wound healing. Adv. Drug Deliv. Rev. *129*, 394–406. https://doi.org/10.1016/j.addr.2018.01.018.
32. Barrientos, S., Stojadinovic, O., Golinko, M.S., Brem, H., and Tomic-Canic, M. (2008). Growth factors and cytokines in wound healing. Wound Repair Regen. *16*, 585–601. https://doi.org/10.1111/j.1524-475X.2008.00410.x.
33. Eming, S.A., Martin, P., and Tomic-Canic, M. (2014). Wound repair and regeneration: mechanisms, signaling, and translation. Sci. Transl. Med. *6*, 265sr6. https://doi.org/10.1126/scitranslmed.3009337.
34. Armstrong, D.G., Swerdlow, M.A., Armstrong, A.A., Conte, M.S., Padula, W.V., and Bus, S.A. (2020). Five year mortality and direct costs of care for people with diabetic foot complications are comparable to cancer. J. Foot Ankle Res. *13*, 16. https://doi.org/10.1186/s13047-020-00383-2.
35. Rehm, M., Huber, H.J., Hellwig, C.T., Anguissola, S., Dussmann, H., and Prehn, J.H.M. (2009). Dynamics of outer mitochondrial membrane permeabilization during apoptosis. Cell Death Differ. *16*, 613–623. https://doi.org/10.1038/cdd.2008.187.
36. Bedoui, S., Herold, M.J., and Strasser, A. (2020). Emerging connectivity of programmed cell death pathways and its physiological implications. Nat. Rev. Mol. Cell Biol. *21*, 678–695. https://doi.org/10.1038/s41580-020-0270-8.
37. Davis, R.J. (2000). Signal transduction by the JNK group of MAP kinases. Cell *103*, 239–252. https://doi.org/10.1016/s0092-8674(00)00116-1.
38. Zhu, S.Y., Zhuang, J.S., Wu, Q., Liu, Z.Y., Liao, C.R., Luo, S.G., Chen, J.T., and Zhong, Z.M. (2018). Advanced oxidation protein products induce pre-osteoblast apoptosis through a nicotinamide adenine dinucleotide phosphate oxidase-dependent, mitogen-activated protein kinases-mediated intrinsic apoptosis pathway. Aging Cell *17*, e12764. https://doi.org/10.1111/acel.12764.
39. Singh, R., Letai, A., and Sarosiek, K. (2019). Regulation of apoptosis in health and disease: the balancing act of BCL-2 family proteins. Nat. Rev. Mol. Cell Biol. *20*, 175–193. https://doi.org/10.1038/s41580-018-0089-8.
40. Hollinger, J.O., Hart, C.E., Hirsch, S.N., Lynch, S., and Friedlaender, G.E. (2008). Recombinant human platelet-derived growth factor: biology and clinical applications. J. Bone Joint Surg. Am. *90*, 48–54. https://doi.org/10.2106/JBJS.G.01231.
41. Li, W., Fan, J., Chen, M., Guan, S., Sawcer, D., Bokoch, G.M., and Woodley, D.T. (2004). Mechanism of human dermal fibroblast migration driven by type I collagen and platelet-derived growth factor-BB. Mol. Biol. Cell *15*, 294–309. https://doi.org/10.1091/mbc.e03-05-0352.
42. Jin, Y., Ding, L., Ding, Z., Fu, Y., Song, Y., Jing, Y., Li, Q., Zhang, J., Ni, Y., and Hu, Q. (2020). Tensile force-induced PDGF-BB/PDGFRbeta signals in periodontal ligament fibroblasts activate JAK2/STAT3 for orthodontic tooth movement. Sci. Rep. *10*, 11269. https://doi.org/10.1038/s41598-020-68068-1.
43. Kramer, F., Dernedde, J., Mezheyeuski, A., Tauber, R., Micke, P., and Kappert, K. (2020). Platelet-derived growth factor receptor beta activation and regulation in murine myelofibrosis. Haematologica *105*, 2083–2094. https://doi.org/10.3324/haematol.2019.226332.
44. Bousoik, E., and Montazeri Aliabadi, H. (2018). Do We Know Jack" About JAK? A Closer Look at JAK/STAT Signaling Pathway. Front. Oncol. *8*, 287. https://doi.org/10.3389/fonc.2018.00287.
45. Vij, N., Sharma, A., Thakkar, M., Sinha, S., and Mohan, R.R. (2008). PDGF-driven proliferation, migration, and IL8 chemokine secretion in human corneal fibroblasts involve

JAK2-STAT3 signaling pathway. Mol. Vis. *14*, 1020–1027.

46. Xu, Q., A, S., Gao, Y., Guo, L., Creagh-Flynn, J., Zhou, D., Greiser, U., Dong, Y., Wang, F., Tai, H., et al. (2018). A hybrid injectable hydrogel from hyperbranched PEG macromer as a stem cell delivery and retention platform for diabetic wound healing. Acta Biomater. *75*, 63–74. https://doi.org/10.1016/j.actbio.2018.05.039.
47. Xu, Q., Guo, L., A, S., Gao, Y., Zhou, D., Greiser, U., Creagh-Flynn, J., Zhang, H., Dong, Y., Cutlar, L., et al. (2018). Injectable hyperbranched poly(β-amino ester) hydrogels with on-demand degradation profiles to match wound healing processes. Chem. Sci. *9*, 2179–2187. https://doi.org/10.1039/c7sc03913a.
48. Zhang, X., Yao, D., Zhao, W., Zhang, R., Yu, B., Ma, G., Li, Y., Hao, D., and Xu, F.J. (2020). Engineering Platelet-Rich Plasma Based Dual-Network Hydrogel as a Bioactive Wound Dressing with Potential Clinical Translational Value. Adv. Funct. Mater. *31*. https://doi.org/10.1002/adfm.202009258.
49. Wang, P., Geng, J., Gao, J., Zhao, H., Li, J., Shi, Y., Yang, B., Xiao, C., Linghu, Y., Sun, X., et al. (2019). Macrophage achieves self-protection against oxidative stress-induced ageing through the Mst-Nrf2 axis. Nat. Commun. *10*, 755. https://doi.org/10.1038/s41467-019-08680-6.
50. Meydan, N., Grunberger, T., Dadi, H., Shahar, M., Arpaia, E., Lapidot, Z., Leeder, J.S., Freedman, M., Cohen, A., Gazit, A., et al. (1996). Inhibition of acute lymphoblastic leukaemia by a Jak-2 inhibitor. Nature *379*, 645–648. https://doi.org/10.1038/379645a0.
51. Dong, Y., Jia, L., Wang, X., Tan, X., Xu, J., Deng, Z., Jiang, T., Rainov, N.G., Li, B., and Ren, H. (2011). Selective inhibition of PDGFR by imatinib elicits the sustained activation of ERK and downstream receptor signaling in malignant glioma cells. Int. J. Oncol. *38*, 555–569. https://doi.org/10.3892/ijo.2010.861.
52. Yan, J., Fu, Z., Zhang, L., and Li, C. (2018). Orai1 is involved in leptin-sensitive cell maturation in mouse dendritic cells. Biochem. Biophys. Res. Commun. *503*, 1747–1753. https://doi.org/10.1016/j.bbrc.2018.07.108.
53. Chen, T., Song, P., He, M., Rui, S., Duan, X., Ma, Y., Armstrong, D.G., and Deng, W. (2023). Sphingosine-1-phosphate derived from PRP-Exos promotes angiogenesis in diabetic wound healing via the S1PR1/AKT/FN1 signalling pathway. Burns Trauma *11*, tkad003. https://doi.org/10.1093/burnst/tkad003.
54. Thery, C., Amigorena, S., Raposo, G., and Clayton, A. (2006). Isolation and characterization of exosomes from cell culture supernatants and biological fluids. Curr. Protoc. Cell Biol. *Chapter 3*. Unit 3 22. https://doi.org/10.1002/0471143030.cb0322s30.
55. Rui, S., Yuan, Y., Du, C., Song, P., Chen, Y., Wang, H., Fan, Y., Armstrong, D.G., Deng, W., and Li, L. (2021). Comparison and Investigation of Exosomes Derived from Platelet-Rich Plasma Activated by Different Agonists. Cell Transplant. *30*, 9636897211017833. https://doi.org/10.1177/09636897211017833.

STAR★METHODS

KEY RESOURCES TABLE

REAGENT or RESOURCE	SOURCE	IDENTIFIER
Antibodies		
Rabbit monoclonal anti-CD31	Abcam	Cat#ab76533; RRID: AB_1523298
Rabbit monoclonal anti-CD9	Abcam	Cat#ab236630; RRID: AB_2922400
Rabbit monoclonal anti-CD41	Abcam	Cat#ab134131; RRID: AB_2732852
Rabbit monoclonal anti-CD63	Abcam	Cat#ab134045; RRID: AB_2800495
Mouse monoclonal anti-CD81	Abcam	Cat#ab79559; RRID: AB_1603682
Rabbit monoclonal anti-Catalase	Abcam	Cat#ab209211; RRID: AB_2612413
Rabbit monoclonal anti-Superoxide Dismutase 1	Abcam	Cat#ab51254; RRID: AB_882757
Mouse monoclonal anti-GAPDH	Abcam	Cat#ab8245; RRID: AB_2107448
Mouse monoclonal anti-VEGF	Abcam	Cat#ab69479; RRID: AB_1271452
Mouse monoclonal anti-PDGFR beta	Abcam	Cat#ab69506; RRID: AB_1269704
Rabbit monoclonal anti-PDGF BB	Abcam	Cat#ab178409; RRID: AB_2268084
Rabbit monoclonal anti-Basic FGF	Cell Signaling Technology	Cat#98658; RRID: AB_398188
Rabbit monoclonal anti-Bax	Cell Signaling Technology	Cat#41162; RRID: AB_2924730
Rabbit polyclonal anti-Cleaved caspase-3	Cell Signaling Technology	Cat#9661; RRID: AB_2341188
Rabbit polyclonal anti-Caspase-3	Cell Signaling Technology	Cat#9662; RRID: AB_331439
Mouse monoclonal anti-Bcl-2	Cell Signaling Technology	Cat#15071; RRID: AB_2744528
Rabbit polyclonal anti-JNK	Cell Signaling Technology	Cat#9252; RRID: AB_2250373
Mouse monoclonal anti-Phospho-JNK	Cell Signaling Technology	Cat#9255; RRID: AB_2307321
Rabbit polyclonal anti-p38 MAPK	Cell Signaling Technology	Cat#9212; RRID: AB_330713
Rabbit monoclonal anti-Phospho-p38 MAPK	Cell Signaling Technology	Cat#4511; RRID: AB_2139682
Rabbit monoclonal anti-JAK2	Cell Signaling Technology	Cat#3230; RRID: AB_2128522
Rabbit polyclonal anti-Phospho-JAK2	Cell Signaling Technology	Cat#3771; RRID: AB_330403
Mouse monoclonal anti-STAT3	Cell Signaling Technology	Cat#9139; RRID: AB_331757
Rabbit monoclonal anti-Phospho-STAT3	Cell Signaling Technology	Cat#9145; RRID: AB_2491009
Rabbit monoclonal anti-α-Smooth Muscle Actin	Cell Signaling Technology	Cat#19245; RRID: AB_2734735
Biological samples		
Sprague Dawley (SD) rats	HFK Bioscience	N/A
Human peripheral blood samples	The First Hospital of China Medical University	N/A
Chemicals, peptides, and recombinant proteins		
AG490	Sigma–Aldrich	133550-30-8
N-Acetylcysteine	Sigma–Aldrich	38520-57-9
STZ	Sigma–Aldrich	18883-66-4
ACD-A	Sigma–Aldrich	8013-89-6
hematoxylin	Sigma–Aldrich	517-28-2
eosin	Sigma–Aldrich	548-24-3
PKH-67	MKBio	MX4023
SP600125	Beyotime	S1876
0.5% crystal violet	Beyotime	C0121

(*Continued on next page*)

Continued

REAGENT or RESOURCE	SOURCE	IDENTIFIER
SB203580	Beyotime	S1863
Enhanced chemiluminescence reagent	Thermo Fisher Scientific	WP20005
Critical commercial assays		
JC-1 kit	Beyotime	C2003S
DCFH-DA probe kit	Beyotime	S0033S
CCK-8	Apexbio	K1018
Annexin V-FITC/PI detection kit	BD Bioscience	556547
24-well Transwell plate	Corning	3422
96-well Transwell plates	Corning	3382
HP-PEG and HA-SH hydrogel	Blafar	N/A
Masson's trichrome	Sigma–Aldrich	1.00485
Revert Aid first-strand cDNA synthesis kit	Fermentas, Life Sciences	K1621
Experimental models: Cell lines		
Human skin fibroblast cell line	The Cell Bank of the Chinese Academy of Sciences	SCSP-106
Experimental models: Organisms/strains		
Sprague Dawley (SD) rats	HFK Bioscience	N/A
Oligonucleotides		
Human-Bax Forward (5′ to 3′): ATCATACTGGTTGCATCTGGTG	This paper	N/A
Human-Bax Reverse (5′ to 3′): CACAGAGGTACGGGCTTATTG	This paper	N/A
Human-Bcl-2 Forward (5′ to 3′): TCGCCGAGATGTCCAGC	This paper	N/A
Human-Bcl-2 Reverse (5′ to 3′): CCCACCGAACTCAAAGAAGG	This paper	N/A
Human-GAPDH Forward (5′ to 3′): GGAGCGAGATCCCTCCAAAAT	This paper	N/A
Human-GAPDH Reverse (5′ to 3′): GGCTGTTGTCATACTTCTCATGG	This paper	N/A
Software and algorithms		
GraphPad Prism version 8.0	GraphPad	https://www.graphpad.com/
Image J	NIH	https://imagej.net/

RESOURCE AVAILABILITY

Lead contact

Inquiries and requests for resources should be directed to and will be fulfilled by the lead contact, Dr. Wenhai Cao (cmudr_cao@163.com).

Materials availability

The study did not generate new unique reagents.

Data and code availability

- All data reported in this paper will be shared by the lead contact upon request.
- This paper does not report original code.
- Any additional information required to reanalyze the data reported in this paper is available from the lead contact upon request.

EXPERIMENTAL MODEL AND STUDY PARTICIPANT DETAILS

Cell culture studies

The human skin fibroblast cell line (HSF) was purchased from the Cell Bank of the Chinese Academy of Sciences (SCSP-106, China), the cell line has been authenticated by STR and tested for mycoplasma contamination. HSF cells were cultured in Dulbecco's modified Eagle's medium (DMEM, Gibco) supplemented with 10% fetal bovine serum (Gibco). The fibroblasts were maintained at 37°C in a humidified atmosphere with 5% CO_2. The cells were subcultured every 2–3 days.

To explore the effects of high glucose (HG) and PRP-Exos, the cells were treated with HG (55 mM), PRP-Exos (50 μg/mL) or both. The cells were subjected to a series of *in vitro* tests at certain intervals. N-Acetylcysteine (Sigma–Aldrich, 38520-57-9), SB203580 (Beyotime, S1863), AG490 (Sigma–Aldrich, 133550-30-8), SP600125 (Beyotime, S1876), imatinib mesylate (Novartis Pharma GmbH, Glivec) and coumermycin A1 (Santa Cruz Biotechnology, 4434-5-3) were used to pretreat the cells for 1 h. N-Acetylcysteine is a ROS scavenger;[49] SP600125 is a specific inhibitor of JNK;[38] SB203580 is an inhibitor of p38 MAPK;[38] AG490 is a specific JAK2 inhibitor;[50] imatinib is an inhibitor of PDGFRβ;[51] and coumermycin A1 is a specific JAK2 activator.[52] The HSFs were cultured in conditioned medium containing N-acetylcysteine (5 mM), SP600125 (10 μM), SB203580 (10 μM), AG490 (50 μM), imatinib (1 μM) or coumermycin A1 (300 nM). After treatment, the indicated experiments were performed on the cells.

Animals

Eight-week-old male Sprague Dawley (SD) rats (HFK Bioscience) between 240 and 280 g were used to induce a diabetic rat model and a subsequent humanized diabetic wound model. Rats were housed in the laboratory of China Medical University and fed *ad libitum* water and rodent diet. All experiments performed on the rats and their care procedures were approved by the Animal Ethics Committee of China Medical University (Approval number: 2020111).

To induce diabetes in SD rats, STZ (Sigma–Aldrich, 18883-66-4) (55 mg/kg) was injected intraperitoneally for one time.[47,53] The establishment of a diabetic model was verified by their blood glucose levels. Blood glucose greater than 16.8 mmol/L lasting for 4 weeks (one test every week) after the injection was considered successful. An electronic blood glucose meter (Roche) was used to measure their serum glucose levels.

The present study involved 12 diabetic rats (12 weeks old; 300–350 g). Initially, the rats were anesthetized with 3.5% isoflurane and maintained at 2%, and four full-thickness excisional wounds (1.5 cm) were created on the back of each rat. There were four wounds on each rat and they were randomized into four treatment groups: control (no treatment), hydrogel (100 μL gel without exosomes), PRP-Exos (200 μg exosomes, subcutaneous injection), and hydrogel/PRP-Exos (100 μL gel containing 200 μg exosomes). The wound was covered with gauze and a bandage. The dressings were refreshed every three days with the standard of care, and wound tissues were sampled and harvested at 7 and 14 days (n=6).

Digital photographs of the wounds were recorded on Days 0, 7, and 14 after the operation (Nikon, Tokyo, Japan). The images of the wounds were measured by ImageJ software. The wound closure rate was calculated as follows: (origin wound area − residual wound area at scheduled time)/origin wound area × 100%.

METHOD DETAILS

Platelet-rich plasma (PRP) extraction

The isolation methods of PRP are based on Tao et al.[17] and Guo et al.[16] All of the blood specimens involved in our study were approved by the ethical committee of the First Affiliated Hospital of China Medical University (Approval number: 2022270). Briefly, we collected totally 40mL peripheral blood samples from healthy volunteers (2 males) and transferred them to tubes containing anticoagulant solution A (ACD-A, Sigma–Aldrich, 8013-89-6) (1 mL of ACD-A/9 mL of blood). Plasma and platelets were collected and transferred to a new centrifuge tube after centrifugation (160 g × 10 min). Then, the plasma was centrifuged again (250 g × 15 min). After discarding the supernatant plasma, the remaining platelet pellets were resuspended to obtain approximately 4 mL of PRP.

PRP-derived exosome (PRP-Exo) extraction

The extraction methods were described by Torreggiani et al.[15] and Thery et al.[54] The PRP samples were centrifuged (250 g × 15 min) to pellet the platelets and then they were washed with PBS (Gibco). After activation with 10% $CaCl_2$ and 1000 U thrombin for 30 seconds (Beyotime, ST1699),[55] the suspension was centrifuged at specific speeds (300 g × 10 min, 2000 g × 10 min), and the debris at the bottom was discarded. As a next step, we filtered the supernatant with a 0.22 μm filter (Millipore) and centrifuged (4000 g × 50 min) it with a 15 ml ultrafiltration centrifuge tube (Millipore). A second ultrafiltration at 4000 g was conducted on the collected liquid after washing it with PBS. To purify the PRP-Exos, the suspension was ultracentrifuged (100,000 g × 70 min). After washing again with PBS, the resuspended PRP-Exos were ultracentrifuged again under the same conditions. Finally, the collected PRP-Exos were resuspended and stored at −80°C.

Identification of PRP-Exos

The concentration and size distribution of the PRP-Exos were measured by Nanosight tracking analysis (NTA; Nanosight, UK). TEM (JEOL, Tokyo, Japan) was used to identify the morphology of PRP-Exos. The biomarkers CD9, CD63, and CD81, cargo bFGF, PDGFBB, and VEGF, and the source marker CD41 were determined by western blotting.

Hydrogel and PRP-Exos-loaded hydrogel preparation

An injectable hydrogel system composed of hyperbranched multiacrylated polyethylene glycol macromers (HP-PEGs) and thiolated hyaluronic acid (HA-SH) reported previously by our team was used in the present study.[46] HP-PEGs and HA-SH were purchased from Blafar (Hangzhou, China). The hydrogel was formed *in situ* via a thiolene click reaction by mixing 100 μL HP-PEG (5% w/v) with 100 μL HA-SH (1% w/v) (both were dissolved in deionized water), and the gelation time was approximately one minute at room temperature. For the PRP-Exos-loaded hydrogel, as the liquid state solution was gently agitated, PRP-Exos were added (1% v/v). After gelation, the gel was injected for further tests.

Exosome uptake by HSFs

After extraction, the PRP-Exos were incubated with PKH67 dye liquor for 5 min following the manufacturer's instructions (MKBio, MX4023). Afterward, to terminate the staining process, 0.5% BSA was added, and the medium was ultracentrifuged (100,000 g × 70 min). After resuspension in PBS, the PRP-Exos suspension was ultracentrifuged again to extract the exosomes. HSFs were incubated with PKH67-labeled exosomes for 24 h, fixed with 4% paraformaldehyde (30 min) and DAPI (5 min) at room temperature, washed with PBS, and finally imaged under fluorescence microscopy.

Cell proliferation assay

A Cell Counting Kit-8 (CCK-8) assay (Apexbio, K1018) was used to evaluate the viability of the HSFs. Briefly, 5×10^3 cells (n = 5 per group) were seeded into 96-well plates. At certain time intervals, a dilution of 1:10 CCK8 solution (10 μL) was added, and the plates were incubated for one hour at 37°C. The absorbance at 450 nm was measured with a microplate reader (ELx800, Bio-Tek), which reflected the viability of the cells.

Cell migration assay

Transwell assays were used to examine the effect of PRP-Exos or HG on fibroblast migration. A total of 1×10^4 cells were placed in the upper chamber of a 24-well Transwell plate (Corning, 8 μm, #3422). The lower chamber was filled with 700 μL medium supplemented with HG or PRP-Exos. The cells on the upper surface of the filter membranes were gently removed by a wet swab after 24 hours of incubation. Then, 0.5% crystal violet (Beyotime, C0121) was applied to stain the filter membrane for 5 min. To evaluate their migration activity, the stained cells remaining on the membrane were observed and counted under a microscope (IX71, Olympus).

Scratch wound assays were also performed. Briefly, HSFs were cultured until 95% to 100% confluence in 6-well plates. The cell monolayer was directly scratched by pipette tips (200 μL). All groups were recorded by microscopy at 24 hours after scratching and washing with PBS. The wound closure area was calculated to determine the level of migration.

Cell apoptosis assay

Fibroblast apoptosis was assessed with an Annexin V-FITC/PI detection kit (BD Bioscience, #556547) following the manual. After specific treatment, HSFs were harvested. For staining, the collected cells were resuspended in 500 μL binding buffer, and then 5 μL propidium iodide (PI) and 5 μL Annexin V-FITC were added to the cells in the dark. After incubation in darkness for 10 min, the cells were detected by flow cytometry (Beckman Coulter).

ROS measurement

Reactive oxygen species (ROS) levels in the HSFs were evaluated by DCFH-DA probe kits (Beyotime, S0033S). After treatment, the cells were incubated with 2,7-dichlorodihydrofluorescein diacetate (DCFH-DA) working solution for 30 min at 37°C in the dark and washed with PBS 3 times. Next, fluorescent images were recorded by a microscope (IX71, Olympus) and analyzed by ImageJ software. Meanwhile, the cells were detected by flow cytometry, and the mean fluorescence intensity represents the level of ROS.

Mitochondrial membrane potential detection

The intracellular mitochondrial membrane potential of the HSFs was assessed with a JC-1 kit (Beyotime, C2003S). The cells were suspended in JC-1 staining solution and incubated for 30 minutes before being washed with JC-1 buffer solution. All procedures were conducted under protection from the light. The resuspended cells were tested by flow cytometry (Beckman Coulter). JC-1 fluorescence was measured at excitation/emission wavelengths of 585/590 (red, aggregate) and 510/527 nm (green, monomer). JC-1 monomer-positive cells (green) were counted to determine the mitochondrial membrane potential.

Western Blot

The lysate of cells or exosomes diluted with loading buffer was heated (95°C, 5 min) and stored at -20°C. Protein extracts were separated with 12.5% sodium dodecyl sulfate–polyacrylamide gel electrophoresis (SDS–PAGE) at 120 volts for 60 minutes and blotted onto a PVDF membrane (Millipore) for 70 minutes at 180 mA. Then, 5% skimmed milk was utilized to block the membranes for 120 min. Primary antibodies were diluted with TBST and incubated with the membranes at 4°C overnight. After washing with TBST, the membranes were incubated with horseradish peroxidase-labeled secondary antibodies (Abcam, ab6721) at 4°C for 1.5 h. An enhanced chemiluminescence reagent (Thermo Fisher

Scientific, WP20005) was applied to visualize the protein bands and imaged by an imaging system (Analytik Jena AG). The optical density was analyzed and normalized to GAPDH with ImageJ software to compare the protein expression levels.

The primary antibodies used included anti-CD9 (Abcam, ab236630, 1:2000), anti-CD41 (Abcam, ab134131, 1:1000), anti-CD63 (Abcam, ab134045, 1:2000), anti-CD81 (Abcam, ab79559, 1:5000), anti-CAT (Abcam, ab209211, 1:1000), anti-SOD 1 (Abcam, ab51254, 1:1000), anti-GAPDH (Abcam, ab8245, 1:10000), anti-VEGF (Abcam, ab69479, 1:1000), anti-PDGFRβ (Abcam, ab69506, 1:1000) and anti-PDGFBB (Abcam, ab178409, 1:1000); anti-bFGF (Cell Signaling Technology, #98658, 1:1000), anti-Bax (Cell Signaling Technology, #41162, 1:1000), anti-cleaved-caspase-3 (Cell Signaling Technology, #9661, 1:1000), anti-Bcl-2 (Cell Signaling Technology, #15071, 1:1000), anti-caspase-3 (Cell Signaling Technology, #9662, 1:1000), anti-JNK (Cell Signaling Technology, #9252, 1:2000) and phosphorylated JNK (p-JNK) (Cell Signaling Technology, #9255, 1:1000), anti-p38 (Cell Signaling Technology, #9212, 1:1000) and phosphorylated p38 (p-p38) (Cell Signaling Technology, #4511, 1:1000), anti-JAK2 (Cell Signaling Technology, #3230, 1:1000) and phosphorylated JAK2 (p-JAK2) (Cell Signaling Technology, #3771, 1:1000), and anti-STAT3 (Cell Signaling Technology, #9139, 1:1000) and phosphorylated STAT3 (p-STAT3) (Cell Signaling Technology, #9145, 1:1000).

qRT–PCR analysis

Total RNA was extracted using TRIzol (Invitrogen, #15596026). A Revert Aid first-strand cDNA synthesis kit (Fermentas, Life Sciences, K1621) was used to synthesize cDNA. Next, qRT–PCR was performed progressively using Gotaq® qPCR Master Mix (Promega Corporation). Relative mRNA expression was calculated using the $2^{-\Delta\Delta Ct}$ method. The results were normalized to GAPDH. The primers used in the present study were as follows: human-Bax: forward, 5′-ATCATACTGGTTGCATCTGGTG-3′, and reverse, 5′-CACAGAGGTACGGGCTTATTG-3′; human-Bcl-2: forward, 5′-TCGCCGAGATGTCCAGC-3′, and reverse, 5′-CCCACCGAACTCAAAGAAGG-3′; human-GAPDH: forward, 5′-GGAGCGAGAT CCCTCCAAAAT-3′, and reverse, 5′-GGCTGTTGTCATACTTCTCATGG-3′.

Cytotoxicity assays

Ninety-six-well Transwell plates (Corning, 8.0 μm, #3382) were used for toxicity testing. These plates ($5x10^3$ cells per well) were seeded with fibroblasts and incubated for 24 and 48 hours. In each of the wells, 20 μL of gel was placed in the upper chamber, and 200 μL of media was added to the lower chamber (n = 5 per group). After indirect contact with the cells, CCK-8 assays were used to test the toxicity of the hydrogels.

Release profile of PRP-Exos-loaded hydrogel

After following the procedure for making PRP-Exos-loaded hydrogel in the previous step, 1% v/v PRP-Exos-loaded hydrogel was prepared with a final concentration of exosomes in the gels of 500 μg/mL. After preparation, 100 μL gel was added to each well of a 24-well plate in 500 μL PBS. Each well contained 50 μg of exosomal proteins. Then, the plate was transferred to an incubator at 37°C and 5% CO_2. At 12, 24, 48, 72, and 96 hours, the supernatant from each well was collected, and after collection, the gels were soaked in fresh PBS. The supernatant collected at each time point was used to determine the protein quantity with a BCA protein quantification kit (Beyotime, P0010).

Histological analysis

A graded series of ethanol and formaldehyde were applied to the wound tissues after they had been sampled at 7 and 14 d, and paraffin was applied to them after they were fixed in 4% formaldehyde overnight. The sections were prepared with a thickness of 5 μm. Then, the prepared sections were treated with hematoxylin and eosin (H&E, Sigma–Aldrich, 517-28-2, 548-24-3) and Masson's trichrome (Sigma Aldrich, 1.00485) and examined under a microscope. The re-epithelialization rate was calculated as follows: (new epidermis length/original wound length) × 100%.

Immunohistochemistry and immunofluorescence analysis

In the immunohistochemical staining procedure, deparaffinized sections of 5 μm thickness were washed with PBS for five minutes. After blocking in 5% serum for 30 minutes, the slides were incubated overnight with primary antibodies against CD31 (Abcam, ab76533, 1:200) and α-SMA (Cell Signaling Technology, #19245, 1:100) at 4°C. For visualization, biotinylated secondary antibodies were applied to stained sections along with avidin-biotin-peroxidase complexes, and DAB substrate was applied to visualize them.

For immunofluorescence staining, rehydrated sections were blocked with 1.5% goat serum and incubated with primary antibodies against CD31 (Abcam, ab76533, 1:100) and α-SMA (Cell Signaling Technology, #19245, 1:100) overnight at 4°C. The nuclei were stained with DAPI (Abcam, ab104139). The images were examined with a confocal microscope (Carl Zeiss, Oberkochen). The number of CD31-positive and α-SMA-positive cells was calculated to indicate vascularization. For each wound sample, five high-power microscopic fields were imaged and evaluated at 400×.

QUANTIFICATION AND STATISTICAL ANALYSIS

In all cases, the data are presented as the means ± standard deviations (SD). Comparisons of the means between the two groups were performed using independent-sample t-tests. The level of significance was determined using GraphPad Prism version 8.0 (GraphPad Software, San Diego, CA) using one-way analysis of variance (ANOVA). Statistical significance was determined by a P value < 0.05.